Lehigh Preserve Institutional Repository

The Effects of Surface Topology of PlasmaporeXP Implants on the Response of Bone Cells

Michael Levin
2021

Find more at https://preserve.lib.lehigh.edu/

This document is brought to you for free and open access by Lehigh Preserve. It has been accepted for inclusion by an authorized administrator of Lehigh Preserve. For more information, please contact preserve@lehigh.edu.

The Effects of Surface Topology of *Plasmapore*^{XP} Implants on the Response of Bone Cells

by

Michael Levin

A Thesis

Presented to the Graduate and Research Committee

of Lehigh University

in Candidacy for the Degree of

Master of Science

in

Bioengineering

Lehigh University

May 2021

© 2021 Copyright

Michael Levin

Acknowledgements

I would like to thank my two advisors, Dr. Himanshu Jain and Dr. Matthias Falk, for their support. I am incredibly thankful to work in a project that tackles real-life problems. I believe this research can help patients live longer and lower their financial strains from having implants, improving hospital settings as a result. In addition, I expanded upon my interest and expertise beyond what I have gathered from the National Institutes of Health (NIH), which I would not have been able to do, had I not been working on this project. In addition to light-sheet microscopes, through this project, I gained more knowledge and expertise in fluorescence microscopy and its various staining techniques. In addition, this was my very first experience to use electron microscopy and its applications. The lab and their project both contributed a lot in increasing my expertise and passion in biomedical research. I believe this project can make an impact to the healthy society.

In addition to my advisors' support, my colleagues in both of these labs also contributed a lot to my progress and this research. When I first came into the lab as Master's student, I received the most support from Caitlyn Hyland. Caitlyn gave me full access to her and Falk's protocol and willingly spent time to train me on some of their techniques, guided me on what supplies and rooms to use, and much more.

The staff members I have worked with helped me with moving this project forward. Dr. Susan Perry, my Bioengineering advisor, made a big contribution to my Master's thesis. She taught me how to design and organize experimental designs with minimal errors, and IF staining analysis. Without her help, I would not have completed this research on time. Lee Graham and Shi-Fang Lu in the Biological Sciences also helped me with finding space for cell culture**,** and we helped each other to make sure our

cells are safe and uncontaminated. I am grateful since the cell culture maintenance is an important factor to my research. Bill Mushock, Robert Keyse, Nikki Rump, Katrina Kraft, Nicole Panebianco, and Lisa Arechiga also gave me valuable support. Bill and Robert helped me with using Lehigh University's electron microscopy facility; they helped me on how to operate them carefully, and even with analyzing some of the data obtained. Nikki, Katrina, Nicole and Lisa helped me with obtaining the Research Assistant (RA) position at Lehigh, which allowed me to be able to work on this great project and assisted with covering tuition for my Master's curriculum.

I would also like to thank Dr. Himanshu Jain, again, and Aesculap, especially Dr. Bob Spiro and Dr. Byron Masi, for funding me by covering my tuition. This support contributes a lot to improving my research progress and to completing my Masters' degree on time. Without their help, I would end up using student loans that I thought could not cover in time.

Lastly, I want to thank my family and friends who have supported me. My grandfather, Igor Garmiz, gave me the biggest support, in terms of encouragement and advising. With his PhD experience at St. Petersburg University ("кандидат наук" in Russian), sharing all of his experiences to me, including his struggles and success, gave much guidance to my research progress. My mother: Irina Garmiz, my father: Dmitri Levin, my sibling: Oscar and Jane Levin, my grandparents, and my little "Настаяши друг," Vasya (a pug) all gave me support that I am very thankful for. I want to also give thanks to my Brazilian Jiu-Jitsu coach, Steve Austin at Sion BJJ, for supporting my pursuit in my Master's degree at Lehigh. Hearing about Steve's knee and hip implants really touched me. Hearing about my research and how much it can impact his life, he constantly cheers for me, which boasts my motivation and my passion for this research tremendously.

Table of Contents

Acknowledgements……..……iv

List of Tables……..…...x

List of Figures……..…….xi

Glossary……xiii

Abstract……..……1

Chapter 1: Introduction……...……..2

Chapter 2: Material Characterization of Plasmapore^{XP} Implants……..……..…11

2.1: Introduction……...……....11

2.2: Materials and Methods……..……..…12

2.2.1: Cutting and sterilizing samples……...……..12

2.2.2: Characterizing samples with Scanning Electron Microscopy (SEM)……...….14

2.2.3: Analyzing elemental composition of samples with Energy Dispersive Spectroscopy (EDS)……..15

2.2.4: Determining surface roughness with a profilometer…….…….16

2.3: Results and Discussion……...……17

2.3.1: Microstructure and composition of Plasmapore^{XP}…….…....17

2.3.2: Surface Roughness comparisons……...……21

Chapter 3: Bone cells interacting with porous Plasmapore^{XP} titanium implants ……..25

3.1: Introduction……..……25

3.2: Materials and Methods……..……...26

3.2.1: Cell Culture……..…….26

3.2.2: Evaluating cell attachment to different substrates using Immunofluorescence (IF) analyses…….……27

3.2.3: Evaluating cell proliferation rate using WST-1 enzyme assay…….……..28

3.2.4: Evaluating cell proliferation using Live/Dead staining and imaging…….….30

3.3: Results and Discussions……..…….32

3.3.1: Adhesion of MG-63 pre-osteoblast cells to different scaffolds……..32

3.3.2: Proliferation rate of MG-63 cells proliferation rate on different scaffolds…..…41

Chapter 4: Conclusions and Future Directions……..……50

4.1: Conclusion of this study……..50

4.1.1: Material characterization of the three investigated materials…..……..…...50

4.1.2: Biological responses related to cellular attachment……..50

4.1.3: Adhesion and cell proliferation to smooth and rough surfaces ……..…...….51

4.2: Future Directions…….……..……..51

4.2.1: Investigate the source of extra carbon and nitrogen in our Plasmapore^{XP} samples ……...…51

4.2.2: Coating of Plasmapore^{XP} to modulate cell/scaffold interactions…….…....52

4.2.3: Investigate cell response related to differentiation……..…….....55

4.2.4: Detecting additional focal adhesion components related to sensing the cellular environment……..……...56

4.2.5: Investigating osteoblasts attached to Plasmapore^{XP} with SEM ……...58

References……..…….59

Vita…….....……69

List of Tables

Table 1: Elemental composition analysis of Plasmapore^{XP}……..……20

Table 2: Surface roughness of flat titanium (“Ti Slug”), PEEK, and Plasmapore^{XP}……..22

List of Figures

Figure 1: Gross (macroscopic) anatomy of bone and its four cell types……...2

Figure 2: Bone-implant osseointegration ……..……..……3

Figure 3: Scheme of bone fracture repair ……....……..…..……..5

Figure 4: Scheme of an intervertebral cage fusing two vertebrae and Aesculap Inc. Arcadius^{XP} L Plasmapore^{XP}-coated spine disk implant ……..6

Figure 5: Aesculap Inc. Arcadius^{XP} L spine disk implant……..……13

Figure 6: Struers Accutom-50 diamond-blade high-speed saw…….…..13

Figure 7: Consolidated SSR-2A-PB autoclave……..……...14

Figure 8: EM/SEM specimen coating – Model EMS575X ……..……....…15

Figure 9: Hitachi 4300 field emission (FE) scanning electron microscope (SEM)……...15

Figure 10: Alpha-Step D-500 stylus profiler from KLA-Tencor…….……..……17

Figure 11: SEM micrographs of Plasmapore^{XP}……..…….……..18

Figure 12: EDS micrographs and elemental composition analyses……19

Figure 13: SEM image of a Plasmapore^{XP} cross-section ….……..……23

Figure 14: Mechanism of enzymatic WST-1 substrate molecule cleavage ……..…29

Figure 15: Human MG-63 osteoblast-like cells growing on glass coverslips ……34

Figure 16: MG-63 cells growing on PEEK……..……35

Figure 17: MG-63 cells growing on flat titanium…….……..……..36

Figure 18: MG-63 cells growing on Plasmapore^{XP}……..……..……37

Figure 19: High-magnification images of MG-63 cells growing on three different surfaces ……38

Figure 20: MC3T3-E1 cells growing on 45S5 Bioglass surfaces……..…..….39

Figure 21: Example of calcein (“Live”) staining of MG-63 cells on 4 different surfaces……...42-43

Figure 22: Another example of calcein (“Live”) staining of MG-63 cells on 4 different surfaces ……..…….44-45

Figure 23: Comparison of linear and semi-logarithmic WST-1 and Live/Dead staining MG-63 cell proliferation curves ….....48

Figure 24: Comparison of MC3T3-E1 and MG-63 bone cells growing on smooth surfaces……..……..53

Figure 25: Comparison of phospho-FAK (focal adhesion kinase) with vinculin (another focal adhesion component) staining ……...56

Figure 26: IF staining of paxillin in HeLa cells ……...……57

Glossary

AA - Amino acid

ACDF – Anterior cervical discectomy fusion

ALP - Alkaline phosphatase

ATCC - American Type Culture Collection

B - New bone formation

BCA - Bicinchoninic acid

BMP - Bone morphogenetic protein

CAMN - Center for Advanced Materials & Nanotechnology

EC - electron coupling

EC-H - EC coupled with hydride (H^-)

ECM - Extracellular matrix

EDS - Energy Dispersive Spectroscopy

EM – Electron microscopy

EMEM - Eagle's Minimal Essential Medium

ESEM – Environmental SEM

Fb - Fibrous tissue

FBS - Fetal Bovine Serum

FE - Field Emission

FEI – Field Electron and Ion Company

HA – Hydroxyapatite

Hc - Haversian canal

IF – Immunofluorescence

IFMD - Institute of Functional Materials and Devices

NADH - Nicotinamide adenine dinucleotide + hydrogen

Oct – Osteocytes

OD – Optical density

PEEK - Polyether ether ketone

Phospho-FAK - Phosphorylated-focal adhesion kinase

pNPP - para-Nitrophenylphosphate

R_a – Linear or “profiling” surface roughness measurement.

RS - mitochondrial succinate-tetrazolium-reductase system

RT-PCR - Reverse transcription–polymerase chain reaction

SBF - Simulated body fluid

SEM - Scanning Electron Microscopy

TAMP - Tailored amorphous multi-porous

TC – Tissue culture

TGF-β - Transforming growth factor-beta

TPS - Titanium plasma-spray

VPS - Vacuum plasma spraying

WST-1 - 4-[3-(4-Iodophenyl)-2-(4-nitro-phenyl)-2H-5-tetrazolio]-1,3-benzene sulfonate

Abstract

Currently, spine disk implants have an average lifetime expectancy of only about 10 years, and the surgical procedures cost about $43,000 on average. Each year, typically 132,000 anterior cervical discectomy fusion (ACDF) surgeries are performed. Titanium is a common metal used for implants because of its corrosion resistance and osseointegration capability. In addition, surface topology affects bone tissue's response towards implants. Prior *in vivo* studies showed that in weeks or months, bone tissues grow and integrate into implants with rough titanium surfaces better than those with smooth titanium surfaces. Our study evaluates how bone cells-alone would respond to smooth or rough titanium surfaces. In addition, stimulating "early endosseous integration" has shown to increase implant's long-term success regarding bone-implant's stability. Thus, our work is to evaluate: 1) bone cell's response to surface topology under *in vitro* conditions, and 2) at time points early after seeding that have not been evaluated previously. Scanning Electron Microscopy (SEM) and Energy Dispersive Spectroscopy (EDS) showed that Plasmapore^{XP}'s surface matches Aesculap's references and that it is mainly composed of titanium. In addition, using our profilometer, we found that Plasmapore^{XP} titanium surface is rough, with R_a value of 17.09 ± 1.17 μm. When seeding MG-63 bone cells onto scaffolds, we found that bone cells adhere less and proliferate at a slower rate on Plasmapore^{XP}'s rough surface than those on smooth titanium surfaces. When evaluating osteoblast cells, they adhere and proliferate less on rough titanium surfaces than on smooth titanium surfaces, which may influence "early endosseous integration" and thus long-term stability.

Chapter 1: Introduction

Understanding bone structure, different types of bone cells, and how cells respond to environmental stimuli are important to better stimulate bone regeneration and to obtain the highest, optimal bone-implant integration. Figure 1 below shows a cross-section of a bone (in the central bone region: diaphysis) and the four, different bone cell types that make up the bone tissue[1].

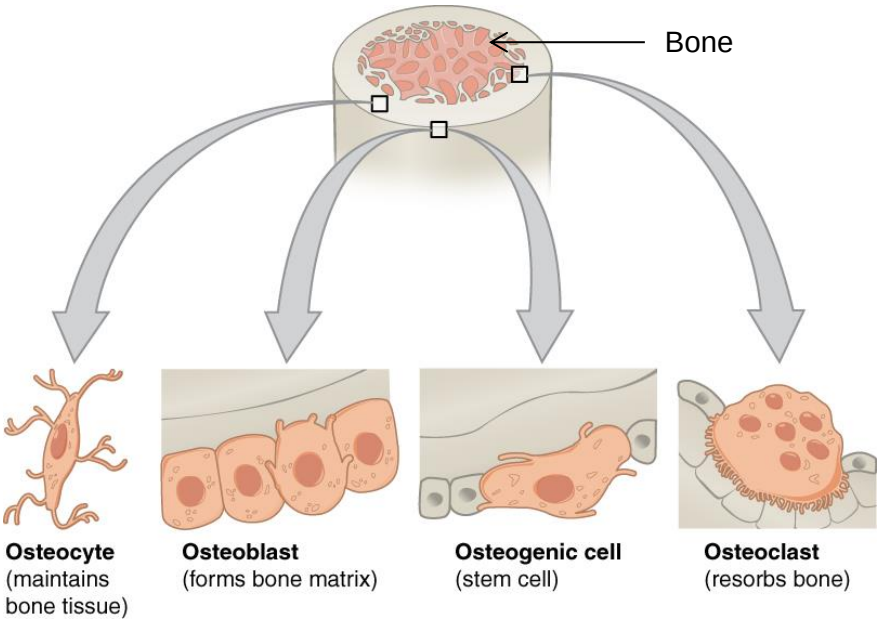

Figure 1: **Gross (macroscopic) anatomy of bone and its four cell types**. Cross-section of a bone in the diaphysis (central bone) region. The four bone cell types and their functions are shown[1].

All bone tissues have these four cell types. Our study focuses on osteoblasts, since our work is focused on bone growth/regeneration, adhesion, and integration towards implants. When osteoblasts "meet" a bone or a favorable material, they would secrete bone matrix to surround them with it, turning into osteocytes. These osteocytes control regeneration, maturation, and resorption, which is critical for fracture healing and osseointegration[1].

Spine implants are used to stabilize the fractured region of the backbone that is caused by trauma or slipped vertebrae, e.g. spondylolisthesis[2]. Sport activities can cause those traumas and elderly people commonly face those issues, both of which are serious enough to require surgery. Spine disk implants are commonly used for these surgeries. When a bone is fractured, it would regenerate and repair itself to fix that problem. One mechanism is for bone tissue to integrate into the implant and strongly bind there to stabilize the fractured region. Implants need to have the right material and its property to stimulate that bone-implant integration, also known as osseointegration. In this process, bone and implant are anchored tightly together without movement or rotation. Figure 2 below is a representative example of bone tissue's stimulated regeneration that would grow towards the implant, integrate with it, and thus bind to it [3].

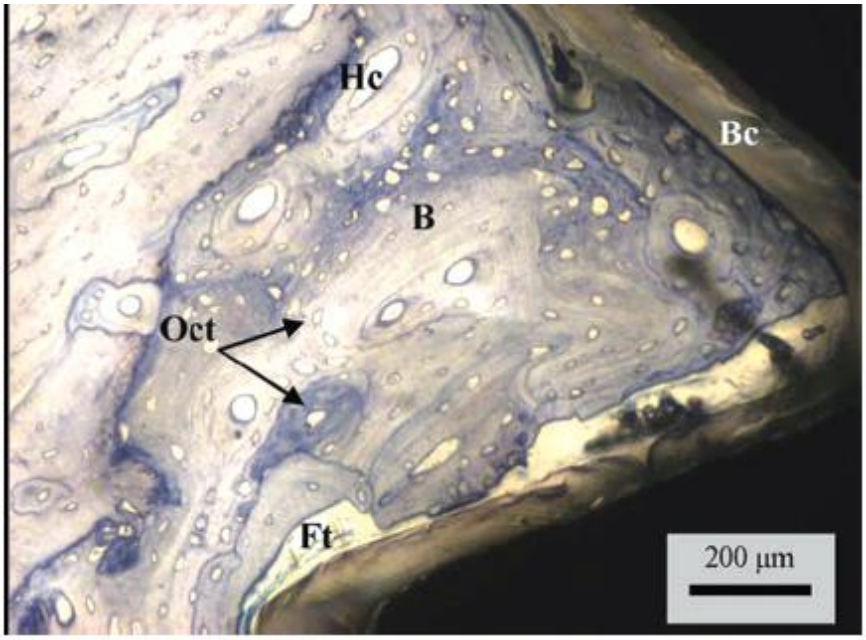

Figure 2: Bone-implant osseointegration. Light microscopic image of the implant's surface (black area on the right) and the "newly formed bone (B)," "osteocyte (Oct) cells," "Haversian canal (Hc)," "Fibrous tissue (Ft)" and "biomimetic coating (Bc)." The overall goal is to stimulate the growth of all cells (except Ft) from the original bone tissue (left region of this image) [3].

The goal for getting most optimal osseointegration is for original bone tissues (left region of Figure 2 image) to stimulate new bone formation bone (B) including osteocytes cells (Oct) and Haversian canal (Hc), while avoiding fibrous tissue (Ft) formation as much as possible. Haversian canal is a microscopic tube that will allow blood vessels and nerves to travel through the canal and communicate with the osteocytes. Fibrous tissue is not a "hard tissue" and it would weaken the bone-implant interfacial strength; it has negative consequences such as "overloading," a term that means loss of bone tissue. Bone would continue integrating into the implant if the bone tissue and the implant share a balanced load-bearing, which stands for how bone and implant transmit mechanical loads in day-to-day activities. If bone tissue bears the entire load, a.k.a. overloading, that tissue would stop integrating, the implant would start loosening and thus causing serious medical consequences. Much research focuses on osseointegration and load-bearing conditions because they impact implant's lifetime expectancy the most.

When a bone fracture (a lesion or injury at the pre-existing bone matrix) occurs, necessary cells including blood, platelets, and biomolecules are recruited and activated to repair it. In order to stimulate bone regeneration for healing, the two fractured parts need to be in contact with each other. Without close contact, bone regeneration does not occur well, and in addition, bone tissues would grow towards each other instead of an outward direction, forming "stumps" on amputated limbs. Once in contact, blood outside of the vessel (hematoma) would start to fill that gap and transform into a callous to connect the two bone fractures together (Figure 3 below) [4]. Once that connection is established, the bone gets remodeled to complete the healing process. Physicians and hospitals want to stimulate that same healing process, including the spine. One established approach to accomplish this result is to use implants coated with metal.

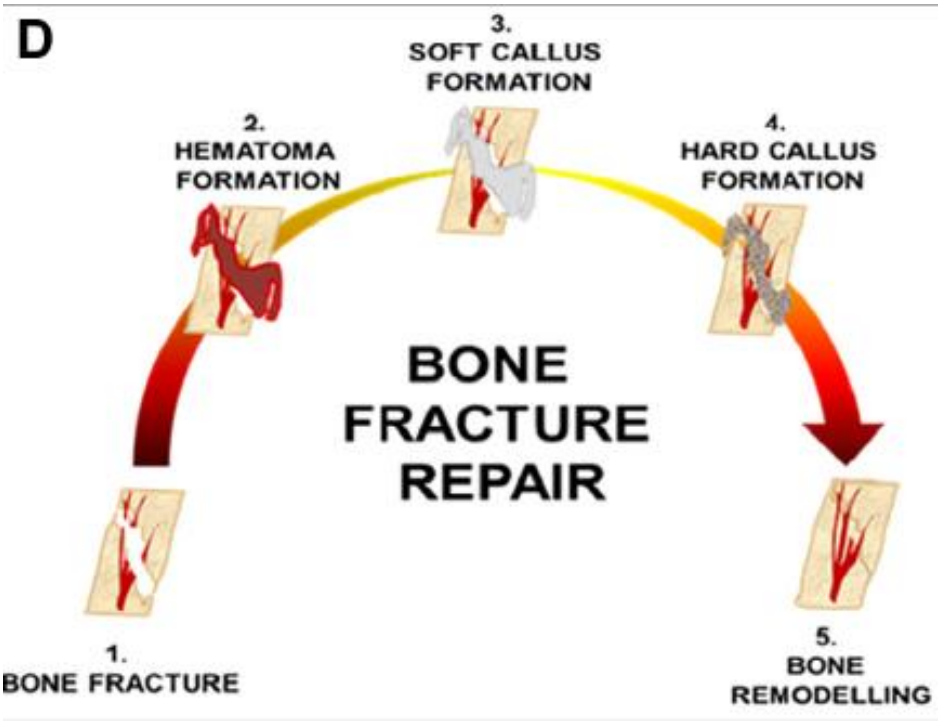

Figure 3: **Scheme of bone fracture repair.** Schematic of how bone regeneration occurs when two bone fracture sites are in contact with each other. When in contact (1.), blood leaks out of wounded vessels and fills the gap in between, creating a hematoma (2.). Once the gap is filled, a callus is formed (from soft to hard) to connect the two bone sites together (3. /4.). Then with remodeling, the two sites are bonded together (5.), healing the bone fracture completely[4].

Currently, implants are either fully metallic or metal only at the surface of another material. That other material is usually plastic, such as polyether ether ketone (PEEK), because it exhibits the same mechanical properties as a bone. Implant ideas were developed in ancient Egypt around 2500 BC, but then the first, dental implant (the only implant at that time) was developed by the Mayans in 600 AD[5]. The materials used in ancient times were gold, ivory, and shells[5]. Later on, other metals beside gold were used, such as chromium, cobalt, iron, steel and eventually titanium[5-6]. Around 1952, Brånemark "accidentally" discovered that his titanium chambers strongly fused with the rabbit's femurs, which then led to the term "osseointegration"[5]. From that point on, titanium has often been used for dental and other kind of implants such as knee, hip, or

spine disk[6]. In addition, titanium has a good, biocompatible property, meaning minimal-to-no foreign body responses, because of its resistance to bodily fluid's corrosion[6]. It can osseointegrate with bone and has a high fatigue life[7-8]. However, there still is significant room for improvement of titanium-coated spine disk implants.

The spine disk implant used in this research project is Plasmapore^{XP} manufactured by Aesculap Inc. It is a hollow cylindrical spinal fusion cage implant, where bone grafts (pieces of bone tissue) are inserted in this hollow space to allow spinal fusion between backbone's two vertebrae[9]. Figure 4 below shows an example of a spinal fusion cage implant inserted in the lumbar (lower back region) spine, with the plate holding those two vertebrae together[10].

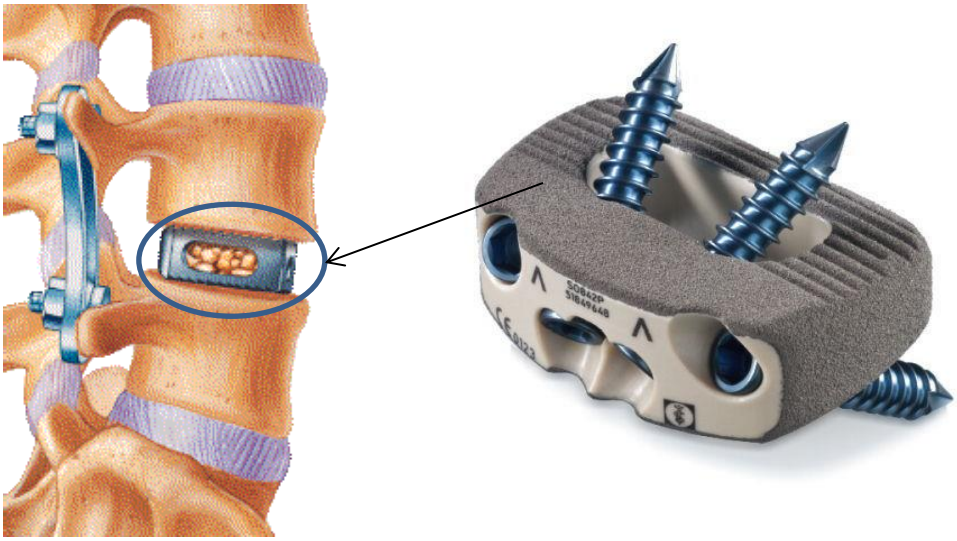

Figure 4: **Scheme of an intervertebral cage fusing two vertebrae and Aesculap Inc. Arcadius^{XP} L Plasmapore^{XP}-coated spine disk implant.** Schematic of an implant cage (circled) used to fuse two vertebrae[10] and the PlasmaporeXP-coated implant being used for fusing two vertebrae[11].

In Figure 4 above, in addition to the cage implant, bone grafts (small bone pieces inside) are also inserted in between the two vertebrae. The goal is to have all bone pieces (bone graft inside the cage and two vertebrae in between) bind to that implant

completely, accomplishing osseointegration and thus having patients function normal life without deliberating back pain. Plasmapore^{XP}'s predecessor, Plasmapore, was tested for Anterior Cervical Discectomy Fusion (ACDF) surgeries, which targeted the spinal neck region[12]. No bone grafts were used in that study. Four years after the operation, based on patient's questionnaire, more people were stating decreased recovery and that pain was resurfacing, potentially indicating Plasmapore implant's lifetime expectancy. Below is the current information regarding Anterior Cervical Discectomy Fusion surgeries:

- Buttermann et. al. states that 10 years after the ACDF operation, using autografts and rigid plate implants (no metal specified), 85-95% of the patients stated that the treatment was successful and that narcotic usage to leverage pain decreased over time[13]. For ACDF surgery, this means that caged implant's lifetime expectancy is at least 10 years if bone grafts are included.
- As of 2018, the cost of ACDF surgery ranged from $39,528 to $47,330[14].
- From 2006 to 2013, 132,000 ACDF surgeries per year were performed in the U.S[15]. With increase of an aging population over time, one can expect this number to increase if no additional improvements on the spine disk implants are made.

Researchers and companies expect that it is possible to increase implant's lifetime expectancy and decrease the number of ACDF surgeries per year. One established approach to this is changing titanium's surface topology.

Recently, Abraham reported that surface characteristics of titanium play an important role in bone integration[5]. Only titanium's surface properties were shown to affect bone cells, no other metals were tested. When coated with titanium, polished or porous surfaces, Cobalt-Chrome-Molybdenum alloy showed better biocompatibility and an increase in adhesion molecule expression than without these coatings[16]. Clinical and

in vivo studies have shown that flat, polished, titanium implants are bio-inert and that they take a long time for bone attachment. When making the implant's surface rougher by e.g. sand-blasting, there was an increase in bone cells and tissue interactions to these implants compared to the implants with flat, polished surfaces, thus stronger bone-implant interface resulted. The fabrication procedure of such improved titanium bone-implant interfaces employs either titanium plasma-spray (TPS) or acid-etch/sand-blasting processes. TPS creates a porous, titanium surface and a larger "roughness" measure on a micro-scale level, while acid-etching/sand-blasting provides "roughness" measure on a nano-scale level. Surface roughness or "roughness" can be numerically measured with a parameter: R_a, which gives a profile or linear roughness measurement, usually in microns or nanometers. R_a means "mean roughness;" it stands for arithmetic average of the heights (peaks and valleys included) across a surface. Prior *in vivo* studies showed that having a mean surface roughness on the order of 100 μm (e.g. 100 - 200 μm) provides the material's interfacial strength that closely matches with the bone's intrinsic strength[17-19]. Lower R_a values showed lower bone-implant interface strength and higher ones were not studied so far[3]. Another study shows that a porous PEEK shows more bone ingrowth and stronger osseointegration than a non-porous PEEK or porous titanium surface[20]. However, all of these studies were performed with animals rather than cells, and their time points were in weeks or months, with 1-2 weeks considered "short term."

Regarding time-points, Klokkevold stated that "early endosseous integration," a.k.a. early osseointegration, are important for the implant's long-term stability with the posterior maxilla dental bone region (upper jaw), to avoid less bone-implant interfacial strength and lower bone density[21]. Spine disk implants may also gain better long-term stability from improving their "early endosseous integration," especially before 3 months.

Since there are very few *in vitro* or shorter time-point (hours to days) studies of bone cell's interactions with the implant, further *in vitro* studies could help medical scientists/physicians determine spine disk implant's "early endosseous integration level" with its bone tissues, thus evaluating long-term success rate. With that said, the present investigation evaluates bone cell's response to titanium surface topology at the cell level *in vitro*.

There are very few studies describing how surface topology of titanium implants affects the response of bone cells. Therefore, present research addresses the effect of Aesculap Inc. Plasmapore^{XP} spine disk implant's surface topology has on bone cells *in vitro*. Once bone cells contact the implant's surface, they undergo either proliferation (cells growing in numbers) or differentiation (maturation of cell type into a more specialized one) process. The two processes normally do not occur at the same time. In fact, there can be an inverse relationship between these two stages. When first interacting with rough surfaces, osteoblast cells respond by producing and secreting more differentiation markers[22]. This correlates to MG-63 cell's response when interacting with Ti-coated PEEK, the combined material composition of Plasmapore^{XP} implants[23]. The majority of studies on evaluating implant's topological surface effects toward bone formation were conducted at the tissue level *in vivo*, but not with respect to cells. Bone will respond differently if the cells were used separately (*in vitro*) or together, like tissues (*in vivo*), since other biological factors like blood vessels, signaling proteins like BMPs (bone morphogenetic proteins) or TGF-β (transforming growth factor-beta), and angiogenesis play a significant role in bone fracture repair[4]. Figure 2 above highlights blood vessel's role in bone fracture repair. Thus, *in vitro* studies can answer questions like: "how do bone cells behave as themselves". On the other hand, *in vivo* studies

would answer: 1) how do bone cells behave when bound together, and 2) what role other factors like angiogenesis, hormones, or signaling molecules play?

In vitro and *in vivo* studies are important for evaluating if the biomaterial in question (e.g. implants, sutures, or valves) is appropriate to be used for treating hospital patients. Ideally, *in vitro* studies were to be done first before *in vivo* studies since they are less expensive than the latter, and they can identify any potential error before moving onto humans or animal models. Our current studies evaluate the effect of surface topology on *in vitro* bone cells regarding attachment and proliferation. They provide greater insight into their properties, e.g. when used in the clinic.

Chapter 2: Material Characterization of Plasmapore^{XP} Implants

2.1: Introduction

Though titanium is biocompatible, its performance can be significantly improved by suitable manipulation of its surface topology[5]. As mentioned in Chapter 1, surface roughness can be numerically measured with a parameter: R_a. As stated from Chapter 1, R_a means "mean roughness;" it stands for arithmetic average of the heights (peaks and valleys included) across a surface. Rough titanium surface tends to stimulate stronger osseointegration or bone-implant's fixation because such surfaces stimulate more bone apposition, which would presumably increase the attachment of bone cells or tissue[24-25]. Roughness is an important property for a micro-textured surface, which is integral to the design of our Plasmapore^{XP} implant - it is significantly higher relative to competing implants[3]. Prior studies showed that having a mean surface roughness on the order of 100 microns (e.g. 100 or 200 μm) makes a material's interfacial strength closely match that of the internal bone[17]. When using the titanium plasma-spray (TPS) coating fabrication method, titanium's surface roughness is typically around 30-50 μm[25]. Aesculap uses a coating fabrication method that is similar to TPS called vacuum plasma spraying (VPS). VPS is TPS done inside a vacuum for samples with high affinity towards gases such as nitrogen or oxygen, which titanium does have[26-27]. Surface roughness properties can be organized based on Wennerberg and Albrektsson's qualitative definitions[8].

- Smooth surface: R_a value <0.5 μm
- Minimally rough surface: R_a value 0.5-1.0 μm
- Moderately rough surface: R_a value 1.0-2.0 μm
- Rough surface: R_a value >2.0 μm

Our goal for this chapter is: 1) to verify Plasmapore^{XP}'s surface topology and elemental composition with the references, and 2) to measure its surface roughness and to compare with the references. This surface roughness measurement could help us predict how bone cells would respond to the implant and the resulting osseointegration.

2.2: Materials and Methods:

2.2.1: Cutting and sterilizing samples

Three types of materials were investigated in this study: PEEK (polyether ether ketone, an organic polymer/plastic), pure, flat titanium samples (Fisher Scientific, Catalog: 4239414 for small slugs or 13999BP for large rods), and Plasmapore^{XP}. For extracting PEEK or Plasmapore^{XP} samples, Aesculap Spine Implant Inc. provided the implant: Arcadius^{XP} L (Figure 5 below). Here PEEK is the main body (tan-colored) and the characteristic of Plasmapore^{XP} implant is its rough, titanium surface that covers the top, sides, behind and the bottom of PEEK's main body. Struers, abrasive, high quality cut-off wheel/saw blade on either Buehler or Struers Accutom-50 high-speed saws (Figure 6 below) were used to cut the implant to its samples for physical, chemical and cell response studies. Diamond or abrasive (e.g. aluminum oxide, Al_2O_3) saws were used for cutting, and water was used as coolant/lubricant. The important parts of using these high-speed saws are feed speed (how fast the blade is moving towards the implant) and wheel resolution speed (how fast the saw turns). These two speeds are important to control in order to avoid damaging the blade or the implant. Since implants are expensive, they were cut down in small pieces to be used for further experiments. Afterwards, they were biologically sterilized by heating to 121°C under 115 kPa pressure in the Consolidated SSR-3A-PB or Consolidated SSR-2A-PB (Figure 7 below) autoclave in "Dry" option for one hour (30 minutes "sterilize" and 30 minutes "dry"). If one does not

choose an option, the autoclave machine would not increase temperature or pressure.

Chemical sterilization of the samples is optional, so it was not done in this study.

Figure 5: **Aesculap Inc. Arcadius^{XP} L Plasmapore^{XP}-coated spine disk implant.** A spine disk implant as shown in Figure 2 without the screws used to hold the insert in place used for experiments performed in this thesis and for treating patients with spine injuries. PEEK core and rough titanium Plasmapore^{XP}-coated surface used and compared in this study are marked[11].

Figure 6: Struers Accutom-50 high-speed diamond-blade saw. This high-speed saw was used to cut Arcadius^{XP} L implants and titanium rods (slugs) into thin, disc-shaped samples[28].

Figure 7: **Consolidated SSR-2A-PB autoclave**. This autoclave was used to sterilize flat titanium, PEEK, and Plasmapore^{XP} samples before their use in experiments with cells in culture.

2.2.2: Characterizing samples with Scanning Electron Microscopy (SEM)

Before imaging with Scanning Electron Microscopy (SEM), samples were sputter coated with iridium using a turbo pumped sputter coater: EM/SEM Specimen Coating – Model EMS575X (Figure 8 below) for 30 seconds to prevent charging. Charged samples could interfere with the quality of the image. Here, sputtering is a technique for depositing materials (usually metal) onto a sample's surface from target cathode by high speed ions. There's a manual provided on how to use this instrument (paper on the left of this image). After sputtering is completed, Hitachi 4300 Field Emission (FE) SEM (Figure 9 below) was used to image a sample's surface in secondary electron mode using 5.0 kV accelerating voltage. The maximum magnification for this SEM is 100,000x. When an electron beam initially hits the sample's surface, various particles are ejected including backscattering and secondary electrons, and x-

rays. In this study, we capture secondary electron emissions for imaging purposes.

Training is required to use this SEM.

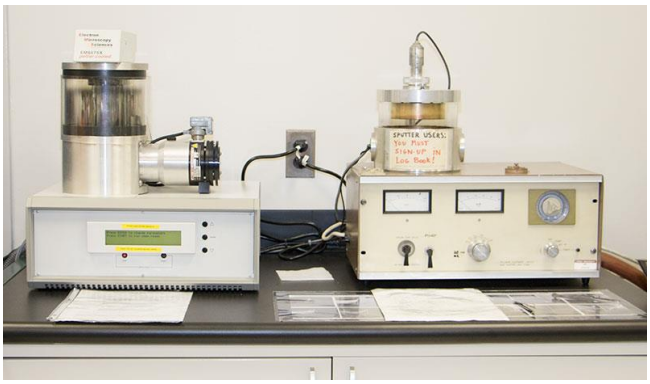

Figure 8: **EM/SEM specimen coating – Model EMS575X.** Specimen Coating was used to sputter coat flat titanium or Plasmapore^{XP} samples with iridium to prevent surface charges[28].

Figure 9: **Hitachi 4300 field emission (FE) scanning electron microscope (SEM).** This microscope was used to obtain 1) scanning electron images or 2) elemental composition spectra of flat titanium or Plasmapore^{XP} samples[28].

2.2.3: Analyzing elemental composition of samples with Energy Dispersive Spectroscopy (EDS)

The secondary electron was used here to obtain the image, and the x-ray emission was used to obtain the elemental composition spectrum. Hitachi 4300 Field Emission (FE) SEM (Figure 9 above) was used for both purposes. After obtaining an electron micrograph through SEM imaging, the EDS scan was obtained yielding composition information from that surface. One important note is that in this analysis either a single point or the whole area of the sample is scanned to collect x-ray emissions. Again, training is required to use EDS spectroscopy.

2.2.4: Determining surface roughness with a profilometer

The surface profiler was used to measure the surface roughness of flat titanium, PEEK and Plasmapore^{XP}'s surfaces. After the sample is cut and sterilized (Materials & Method's 2.2.1 section), one of those three materials are placed and anchored inside the profiler (Figure 10 below). Alpha-Step D-500 stylus profiler from KLA-Tencor was used to measure this surface roughness, located in C348 at Iacocca Hall. This instrument comes with a software program, with these steps to follow:

1) Move the stage down until the needle interacts the sample. The needle inside this instrument was moved down until touching the material being studied.
    a. Avoid breaking or damaging the sensitive needle when moving it down.
2) Set "scan parameters" on the needle. Before "profiling a sample" (running the instrument), one needs to control and check the conditions in that "scan parameters" in order to obtain desirable data. The important conditions are "Speed" of the needle's movement, "Length" of the measurement, "Range" of the

surface roughness's peaks-and-valleys, and "Stylus force" of the needle pressing onto the sample.

3) Start the surface roughness reading experiment, and record it.

This instrument measures surface roughness by placing its needle on the sample's surface, moving in a linear fashion, and record its roughness: R_a. R_a is used to compare different samples and all the results are reported in nanometers (nm). This profiler can give surface roughness measurements in microns or nanometers. The needle used here is very expensive, thus extra precautions should be taken.

Figure 10: **Alpha-Step D-500 stylus profilometer.** This instrument was used to measure surface roughness parameter, R_a, of flat titanium, PEEK, and Plasmapore^{XP} surfaces[29].

2.3: Results and Discussion

2.3.1: Microstructure and composition of Plasmapore^{XP}

We have obtained scanning electron microscope (SEM) images or micrographs of the Plasmapore^{XP} implants as shown in Figures 11B and 11D. Our SEM and published article's images (Figure 11A and 11C) are very similar, confirming previous analysis.

Plasmapore^{XP} used in Cheng. et. al. (2018) Plasmapore^{XP} used in this study

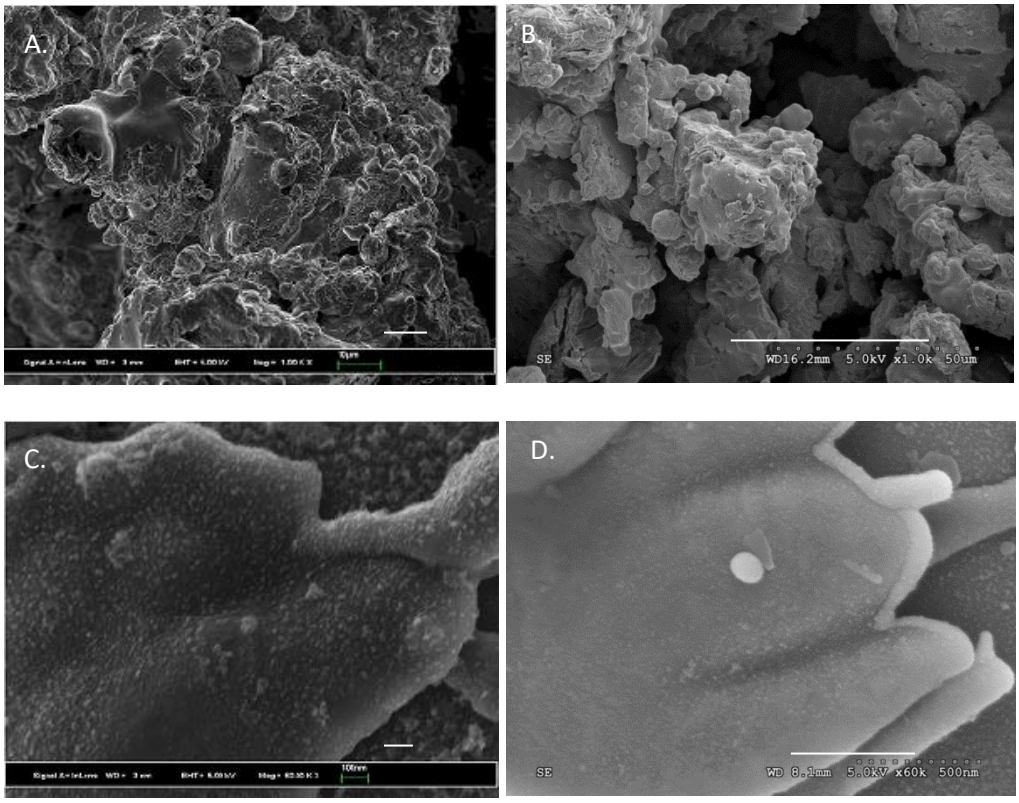

Figure 11: SEM micrographs of Plasmapore^{XP}. Comparison of the micrographs of Ti-PEEK (Plasmapore^{XP}'s material) taken from Cheng et al.[22] (A and C) and Plasmapore^{XP} samples (B and D) used in this study. Magnification 1,000x for (A) and (B), and 60,000x for (C) and (D). Scale bars: A: 10 µm; B: 50 µm; C: 100 nm and D: 500 nm.

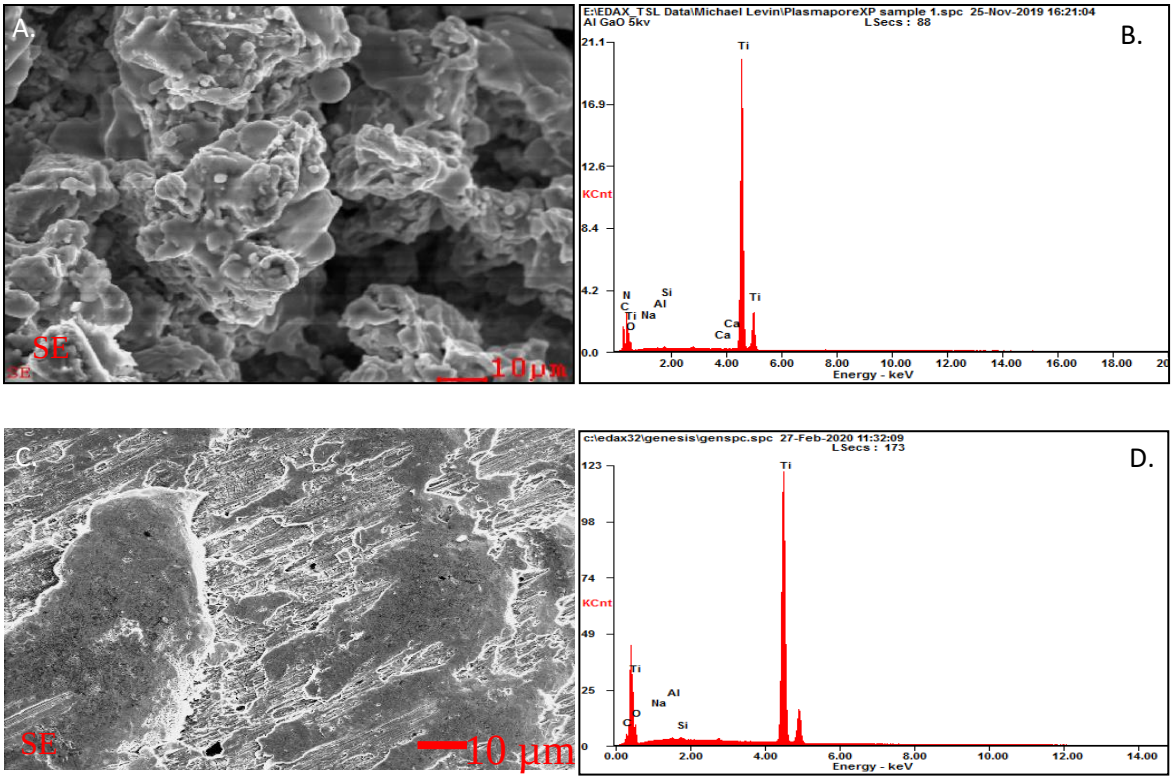

Figure 12: **EDS micrographs and elemental composition analyses.** Region of our Plasmapore^{XP} (Figure A) used to provide the elemental composition (Figure B). Also shown is a region of flat titanium (Figure C) used to provide its elemental composition (Figure D).

Element	Notation	C	O	N	Na	Al	Si	Ca	Ti
Atomic Percentage of Plasmapore^{XP} (%)	A	30.9	9.5	17.2	0.6	0.2	0.3	0.09	42.5
Atomic Percentage of flat titanium (%)	B	13.2	23.2	0	0	0.5	0.4	0	62.8
Recalculating Atomic Percentage of Plasmapore^{XP} (%) without extra carbon	C	0.0	9.5	17.2	0.6	0.2	0.3	0.09	73.4
Recalculating Atomic Percentage of flat titanium (%) without extra carbon	D	0.0	23.2	0	0	0.5	0.4	0	76.0

Table 1: **Elemental composition analysis of Plasmapore^{XP}.** Atomic percentage of each element (in K-shell excitation) gathered from the EDS spectrum in Figure 12. 20.0 kV accelerating voltage was used for Plasmapore^{XP} sample (A), and 15.0 kV for flat titanium sample (B). Recalculation (C) was done by the assumption that all extra, contaminated carbon in Plasmapore^{XP} is removed. Recalculation (D) was done by the assumption that all extra, contaminated carbon in flat titanium is removed.

The chemical analysis of EDS instrument would collect that resulting x-ray emission to produce the elemental composition spectrum shown in Figures 12B and 12D, and Table 1 here. A region of Plasmapore^{XP} (Figure 12A) was scanned to obtain its typical elemental composition information (Figure 12B) and a region of pure, flat titanium (Figure 12C) was scanned to obtain its elemental composition information (Figure 12D). For Figures 12A and 12C, the whole image was scanned for collecting x-ray emission. The energy of these x-ray emissions indicates how much energy was used to eject an electron from the K-shell, which dictates the element types based on those K-shell energies. When collecting all x-ray emission energies, the program compiled the list of elements detected and the intensity of peaks ("kCnt," kilo counts) yielded composition in atomic (or weight) percentage (see Table 1). These data are the first analyses of Plasmapore^{XP} implants obtained by EDS**.**

Titanium has the largest concertation of elements present in both Plasmapore^{XP} and flat titanium. However, the data also shows that Plasmapore^{XP}'s surface has significant carbon (30.9%) and nitrogen (17.2%). These elements are not expected based on the description available from the manufacturer. The analysis of flat titanium also showed significant carbon (13.17%). We believe that carbon resulted from contamination during deposition of conducting film or analysis in the SEM. The carbon concentration on flat titanium is small compared to Plasmapore^{XP}, which could have resulted from contamination from underlying PEEK in the probed volume. If the extra, contaminated carbon was removed from Plasmapore^{XP} and flat titanium (Table 1C and 1D), their calculated titanium would match each other. Oxygen is from native TiO_2, which is inevitably present on titanium surfaces exposed to air. A lower concentration of oxygen on Plasmapore^{XP} (9.5%) compared to on flat titanium (23.19%) indicates a thicker oxide layer on the latter type sample.

The presence of nitrogen in Plasmapore^{XP} sample at 17.2 atomic percentage (%) is very intriguing. The details of its fabrication process are not available, but according to information in open literature, the rough, porous titanium coatings on PEEK are fabricated in vacuum. However, the quality of vacuum is not known, and it is possible that there was residual air or nitrogen in the chamber, which ended up as a thin nitride coating on the sample. Some of the carbon could also result from the manufacturing process. Regardless, Plasmapore^{XP}'s low titanium concentration is due to unexpected carbon and nitrogen as contaminants. A confirmation of this analysis is warranted from EDS measurements on multiple samples.

With regard to the porous morphology of Plasmapore^{XP} surface, the SEM micrographs in Figures 11 and 12, yield the pore's diameter around 50-100 µm, which is close to Aesculap's reference value: 60-150 µm[11]. One important note is that our

measured range is based on 3 sample sizes, n = 3, which could make our measurement inaccurate.

2.3.2: Surface Roughness comparisons

Table 2A-C below is the output from using this profiler instrument and Figure 13 is Plasmapore$^{XP'}$s cross-section imaging.

A.

	Z(M) - Z(R) (nm)	Ra (raw) (nm)	Rq (raw) (nm)	Rt (Pk-Vly) (nm)	Radius (mm)
Ti Slug, left side, Least Squares	404.00	500.36	689.27	4,822.5	12,549
Ti Slug, middle, Least Squares Fit	861.32	611.25	772.74	4,680.5	24,239
Ti Slug, right side, Least Squares	1,807.0	514.30	652.32	3,915.5	10,754
Average	1,024.1	541.97	704.78	4,472.8	15,847
StdDev	715.526	60.402	61.689	487.859	7,322.606

Real Time Display | Cursor Control | Scan Parameters | Data Analysis Results - Multiple Window

B.

	Z(M) - Z(R) (nm)	Ra (raw) (nm)	Rq (raw) (nm)	Rt (Pk-Vly) (nm)	Radius (mm)
PEEK, left side, Least Squares Fit	-3,659.1	1,677.0	2,096.9	11,832	464.97
PEEK, middle, Least Squares Fit	-655.70	2,086.4	2,513.1	11,263	366.12
PEEK, right side, Least Squares	-5,440.4	2,533.2	3,160.2	16,635	301.11
Average	-3,251.7	2,098.9	2,590.1	13,243	377.40
StdDev	2,418.222	428.236	535.812	2,951.015	82.51

Real Time Display | Cursor Control | Scan Parameters | Data Analysis Results - Multiple Window

C.

	Z(M) - Z(R) (nm)	Ra (raw) (nm)	Rq (raw) (nm)	Rt (Pk-Vly) (nm)	Radius (mm)
PlasmaporeXP, left side, Least	-46,299	15,930	19,307	1.0281e+5	158.14
PlasmaporeXP, middle, Least	-27,647	18,265	22,237	1.2974e+5	872.13
PlasmaporeXP, right side, Least	-24,569	17,081	20,469	1.0428e+5	2,888.4
Average	-32,838	17,092	20,671	1.1228e+5	1,306.2
StdDev	11,758.43	1,167.539	1,475.408	15,141.54	1,415.948

Real Time Display | Cursor Control | Scan Parameters | Data Analysis Results - Multiple Window

Table 2: **Surface roughness of flat titanium ("Ti Slug"), PEEK, and Plasmapore^{XP}.** Surface roughness of each material: flat titanium (Figure A), PEEK (Figure B) and Plasmapore^{XP} (Figure C) based on profilometer measurements. On average, determined Ra values using this instrument for flat titanium was 542.0 ± 60.4 nm (0.5420 ± 0.0604 µm), PEEK 2,099.0 ± 428.2 nm (2.0990 ± 0.4282 µm) and Plasmapore^{XP} 17,092 ± 1,167.5 nm (17.092 ± 1.1675 µm).

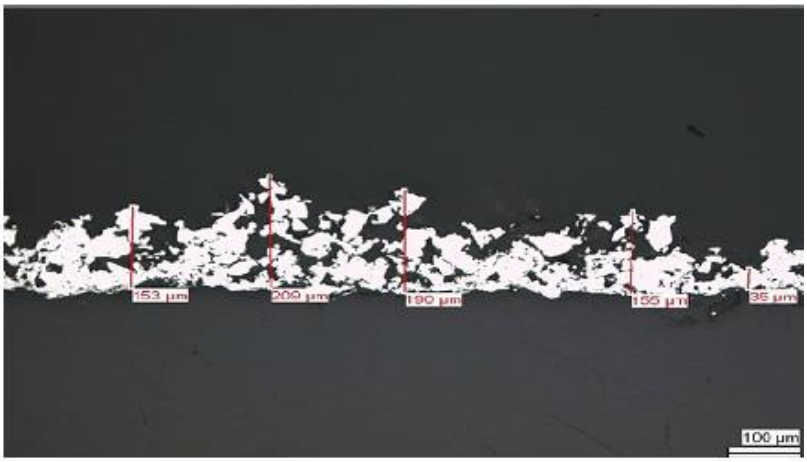

Figure 13: **SEM image of a Plasmapore^{XP} cross-section.** A cross-section of Plasmapore^{XP}'s titanium surface showing its porous titanium coat structure and thickness[22].

When making measurements, we found that flat titanium's R_a value is 0.5 ± 0.06 µm, PEEK's R_a value is 2.1 ± 0.4 µm and Plasmapore^{XP}'s R_a value is 17.1 ± 1.2 µm. Using Wennerberg and Albrektsson's standards, flat titanium is between "smooth" and "minimally rough" surface category, PEEK is between "moderately rough" and "rough" surface category, and Plasmapore^{XP} is in the very "rough" surface category. With that said, Plasmapore^{XP} has a very rough surface, qualitatively speaking.

Despite the implant's titanium surface being technically "rough," the tested sample may not be rough enough. In one report, TPS fabrication yielded porous, titanium surface to be 30-50 µm rough[25]. In another report, Aesculap reported producing three implants by TPS method, which had surface roughness to be higher than 100 µm instead: 101, 175, and 103 µm[17]. In that study, Pröbster inserted these implants into rabbit's femur and showed that their tensile interface strength closely matched with that of the rabbit bone. The author concluded that 100-200 µm surface roughness was common for TPS coating; and TPS-coated implants with "mean surface roughness of the order 100 µm" had interface strength closely matching with internal bone strength[17]. This

would indicate that titanium's surface roughness in 100 μm range (e.g. 100 or 200 μm) would stimulate osseointegration. Based on this information and measurements on one specific sample, it is likely that Plasmapore^{XP}'s surface may not be "rough enough" to stimulate osseointegration. Obviously, multiple samples need to be characterized with a more detailed analysis of 3D porosity.

Based on Plasmapore^{XP}'s cross-section imaging (Figure 13), one possibility of our implant's low R_a measurement is that the needle did not go into those pores deep enough, thus did not obtain all the information for a complete analysis[23]. The profiler's surface roughness measurement depends on needle's penetration. Looking at the cross-section image, it is only possible for the needle to probe the porous titanium's superficial part of the coating. It is impossible for the needle to physically go deeper and into the crevices and pockets, which could have provided more relevant information on Plasmapore^{XP}'s R_a value.

Chapter 3: Bone cells interacting with porous Plasmapore^{XP} titanium implants

3.1: Introduction

First contact with the material dictates bone cell's behavior. We know that surface topology and elemental composition can affect bone tissue's behavior. Titanium was known to be biocompatible, which makes it a reliable choice for implant's surface coating to interact with bone tissues. Moreover, numerous studies show that rough titanium surface stimulates more bone regeneration and fixation[3, 5, 8, 17-19, 22-25]. In addition, porosity stimulates stronger bone fixation[19]. However, all of these studies are in regards to bone as a tissues and not concerning bone cells.

Here, I have evaluated how bone cells (osteoblasts) behave and respond when they begin to interact with a given implant's rough, porous titanium surface. We implemented *in vitro* conditions and an experimental timeframe of hours to days. When bone cells first interact with a given material, the first parameter to evaluate is potential cytotoxicity, which is evaluating if the cells would survive and thrive on that surface. The next step includes evaluating whether bone cells are triggered to regenerate. For *in vitro* studies, that would be based on cellular proliferation and differentiation (changing from one cell type to another, usually more specialized like mature bone cells). In prior studies, Plasmapore^{XP}'s titanium surface was shown to promote cell differentiation rather than cell proliferation[23]. In addition, in their *in vivo* studies, they showed that an implant with coated, porous titanium surface has a higher pull-out strength and an increased ability of new bone formation than one without that coating[23]. For our *in vitro* studies, instead of pull-out strength, we evaluated cellular adhesion; and instead of new bone formation, we evaluated cellular proliferation. In this project, we also aimed to investigate

why bone cells adhere or proliferate less well on Plasmapore^{XP}'s surface compared to canonical surfaces such as tissue culture (TC) plastic, or protein-coated glass coverslips by investigating cell behavior within hours to days after seeding.

3.2: Materials and Methods

3.2.1: Cell Culture

Cell culture means to grow cells in controlled conditions by 1) feeding and replacing old-to-new "food" (= culture media) and 2) by controlling the cell population. L-Glutamine and Fetal Bovine Serum ("FBS") needed to be added as media's extra supplement and Penicillin-Streptomycin needed to be added to minimize bacterial infection and colonialization. The latter case is done by "passing:" detaching all the cells ("trypsinization" with Trypsin-EDTA) and placing ("seeding") a portion of the total number of cells onto the new plate and re-grow from there. This needs to be done only when cells are almost-to-completely confluent (80-100% "confluency") on the dish.

Human MG-63 osteosarcoma cell line (CRL-1427; American Type Culture Collection [ATCC], Manassas, VA, USA) were cultured in 60 mm-diameter tissue culture plates. Cells were pooled from 2.0 mL cryogenic tubes in liquid nitrogen or -150 °C. The media used was Eagle's Minimal Essential Medium (EMEM) (ATCC, Manassas, VA, USA, Cat. # 30-2003), with 50 mL of it removed and then supplemented with 50 mL of 10% FBS (R&D Systems, Minneapolis, MN, USA, Cat. # S11150), 3 mL of Gibco^{TM} L-Glutamine (200 mM) (Fisher Scientific, Nazareth, PA, USA, Cat. # 25030081) and 5 mL of Gibco^{TM} Penicillin-Streptomycin (Fisher Scientific, Nazareth, PA, USA, Cat. # 15070063). The EMEM media has 500 mL volume limit and adding 50 mL more of any liquid would cause over-spilling and thus contamination. This volume limit is why 50 mL of EMEM was removed, to give room for 50 mL of 10% FBS nutritional supplement to be

added in. Media exchanges occur every 48 hours. Cells were cultured until reaching confluency on that dish, usually in 5-7 days. After that, cells were passed using Gibco™ Trypsin-EDTA (0.25%) phenol red (Fisher Scientific, Nazareth, PA, USA, Cat. # 25200056) and EMEM media.

When used for biological experiments, cells were seeded at 10,000 cells/cm^2 (approximately 1:10 to 1:20 split ratio) in order to reach confluency by 5-7 days. The dishes used were either 35 mm-diameter or 60 mm-diameter tissue culture, 6-well or 96-well plates. Cells were counted using a hemocytometer.

3.2.2: Evaluating cell attachment to different substrates using Immunofluorescence (IF) staining and imaging

Cellular adhesion can be evaluated through Immunofluorescence (IF) staining and imaging. IF is when antibodies ("Immuno-") and fluorescence (adding color in imaging) are involved for staining. There are two goals for IF staining. One is to label nuclei to indicate cell's presence. Another is to evaluate if the biomolecules involved in cellular adhesion are present and to detect their morphology. In this study, those biomolecules are focal adhesions (through vinculin staining) and actin (cytoskeleton interacting with focal adhesions). Cells were processed for analysis by fluorescence detection of nuclei by incubating in DAPI (Molecular Probes, Eugen, OR, Cat. # D1306), actin using Alexa488 (or Alexa568)-phalloidin (Molecular Probes, Grand Island, NY, Cat. # A-12379), and vinculin and phospho-FAK using immuno-staining (mouse monoclonal antibody-Sigma, St. Louis, MO, Cat. # V9131 for anti-Vinculin and rabbit polyclonal antibody-Sigma, St. Louis, MO, Cat. # V9131 for phospho-FAK). Stains and antibody concentrations are described in the next paragraph, through dilutions like "(1:100)." DAPI and phalloidin are molecular probes to which a chromophore is covalently bound, thus

only need one incubation step; vinculin, and phospho-FAK staining involves primary and secondary antibodies, thus require two incubation steps. Vinculin staining would be used and evaluated for Chapter 3 while phosphor-FAK would be introduced in Chapter 4.

In brief, cells were fixed using 3.7% formaldehyde in 15 minutes and at room temperature, followed by permeabilization with 0.2% Triton X-100 in 15 minutes and at room temperature for staining with vinculin. Cells were then blocked in 5% BSA/PBS at room temperature for 1 hr. or overnight. Fixation is to preserve cells and their cellular components; permeabilization is to allow large molecules such as antibodies to enter into the cell's body; blocking is to prevent antibodies to bind non-specifically which increases unspecific background staining. The primary antibodies were diluted in blocking solution to 1:300 or 1:500 and incubated with cells at room temperature for 1 hr or 4°C overnight. Blocking solution containing DAPI (1 µg/ml), Alexa488 (or Alexa568)-phalloidin (1:100) and secondary antibody (1:300 or 1:500), Alexa488-conjugated goat-anti-mouse (Molecular Probes/Invitrogen, Grand Island, NY, Cat. # A11031) for vinculin was incubated with the cells at room temperature for 1 hr or 4°C overnight. Coverglasses were mounted by submersing into 50 µL of SouthernBiotech^{TM} Fluoromount-G^{TM} Slide Mounting Medium onto a microscopic slide (with the cell side facing bottom), and then sealed with nail polish. Scaffolds (flat titanium discs, PEEK, and Plasmapore^{XP}), samples were imaged by submersing them in 50 µL of SouthernBiotech^{TM} Fluoromount-G^{TM} Slide Mounting Medium onto a glass bottom 35-mm tissue culture dish with the side on which cells were seeded facing the glass bottom. Imaging was performed using a Nikon Eclipse TE2000-U inverted fluorescence microscope and its SPOT Advanced v5.1 software program.

3.2.3: Evaluating cell proliferation rate using WST-1 enzyme assay

WST-1 is a tetrazolium salt that is cleaved on the cell's surface to turn into formazan. Figure 14 below shows the mechanism of how WST-1 is cleaved into formazan to produce the darker red color for absorbance reading.

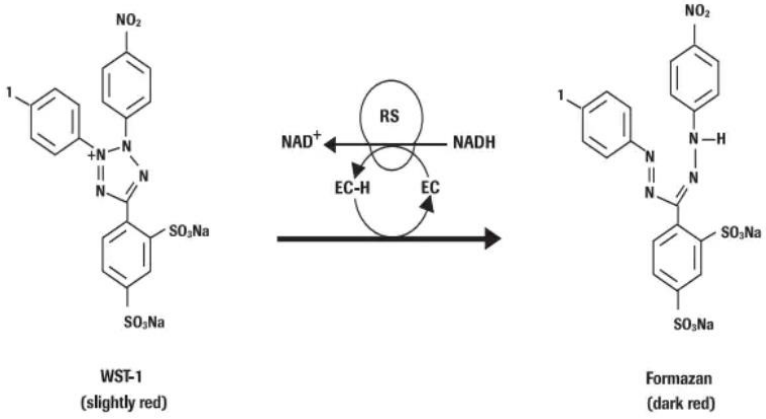

Figure 14: **Mechanism of enzymatic WST-1 substrate molecule cleavage**. Mechanism of cleaving tetrazolium salt WST-1 (4-[3-(4-Iodophenyl)-2-(4-nitro-phenyl)-2H-5-tetrazolio]-1,3-benzene sulfonate, colorless) into colored formazan. Note: EC = electron coupling, EC-H = EC coupled with hydride (H^-). RS = mitochondrial succinate-tetrazolium-reductase system and NADH = Nicotinamide adenine dinucleotide (cofactor critical for metabolism) (Sigma Aldrich, Product #: CELLPRO-RO).

The cleavage process depends on the glycolytic production of NAD(P)H in viable cells. The product, formazan, produces red color, and the amount of formazan produced correlates to the red-color intensity. Plate/microplate reader illuminates a light source with a specific wavelength into the 96-well plate's well and the light detector on the other side absorbs and measures how much of the incident light was transmitted through the well's sample[31]. For WST-1 assay, the wavelength for our microplate reader was set to 450 nm, which would indicate the number of formazan products produced and thus number of viable cells present in solution. Thus, higher OD 450 nm reading indicates

more formazan produced, which means more viable cells are present in that solution. This assay was used for evaluating cellular proliferation, though indirectly because cells are not directly counted.

For this study, after reaching confluency in the 60 mm-diameter tissue culture plate, cells were trypsinized and seeded into 96-well plate in 10,000 cells/cm^2. Four columns were used to dictate the time points: 1, 4, 5, and 6 days after seeding and the rows represent either MG-63 cell's standard curve, cells alone or cells on top of any of the three scaffolds: PEEK, flat titanium, and Plasmapore^{XP}. The standard curve and each scaffold sample were in triplicates (n = 3 sample size) so that their average and standard deviation can be calculated. The reagent was WST-1 (Sigma Aldrich, Milwaukee, WI, USA, Cat. # 11644807001) for the WST-1 assay. This assay can be applied for cell proliferation, viability, and cytotoxicity. 3-4 hours of incubation was done to get the accurate absorbance reading. Absorbance at OD 450 nm was read, subtracted by the reference wavelength: OD 600 nm on the Tecan Infinite M200 Pro Plate reader.

For this proliferation study, duplication time for each sample is necessary to compare their proliferation rate on each other. For duplication time calculations, the Sciencing website on calculating cell doubling by Sean Butner was used[30]. The idea here is that from "Day 1" to the later days counted for each sample, one uses logarithm to the base of 10 (e.g. log (10) = 2) and log (2) in order to obtain number of generations per number of days. Afterwards, one inverts it to obtain number of days per generation, which are the numbers used here to evaluate MG-63 cell's proliferation rate.

3.2.4: Evaluating cell proliferation using Live/Dead staining and imaging

Live/Dead is a staining kit that contains two staining components: calcein-AM ("Live") and ethidium homodimer-1 ("Dead"). Calcein-AM stains cell's active, intracellular esterase activity, which is functionally active only on viable cells thus considered "Live." In addition, it will label the whole cell body and sometimes intensity changes. This can provide cell morphology information in addition to being "live" or not. When a cell undergoes mitosis for example, their body changes from epithelial-like pattern to circular and it becomes brighter under the microscope. The emission color for that stain is green. Ethidium homodimer-1 stains the cell only when their plasma membrane's integrity is lost, meaning a damaged membrane like a leakage. Having a damaged membrane that allows ethidium homodimer-1 to pass through is why they're considered "Dead." The emission color for that stain is red. Combining these two stains can provide cell viability or cytotoxicity information when in contact with the sample. In addition, this staining kit was used for evaluating cellular proliferation directly.

For this study, after reaching confluency in the 60 mm-diameter tissue culture plate, cells were trypsinized and seeded into 6-well plate for scaffolds and 35-mm diameter tissue culture dish as TCP, both in 10,000 cells/cm^2. The stain used is Invitrogen™ LIVE/DEAD™ Viability/Cytotoxicity Kit, for mammalian cells (Fisher Scientific, Nazareth, PA, USA, Cat. # L3224). For every 10 mL of 1xPBS used, 5 µL of Calcein and 20 µL of Ethidium Homodimer-1 were used to create the solution; smaller or larger volumes follow accordingly. The cells on the scaffolds or the tissue culture dish were imaged after 15-20 minutes of incubation at room temperature. Imaging was performed using a Nikon Eclipse TE2000-U inverted fluorescence microscope and its SPOT Advanced v5.1 software program.

Just like in WST-1 assay's proliferation study, duplication time for each sample is necessary to compare their proliferation rate on each other. Regarding calculations, MG-63 cells were directly counted on each image, though counting by computer programming such as ImageJ or Python is advisable in order to minimize time doing the task. Usually, a programming technique such as segmentation would be involved. Each sample per time point has 3 representative images. Once all 3 representative images per sample and time point where counted, average and standard deviation for each 3 representatives per sample and time point would be calculated. For duplication time calculations, the Sciencing website on calculating cell doubling by Sean Butner was used here[30]. The idea is that from seeding (100 cells/mm^2 in "Day 0") to the days counted for each sample, one uses logarithm in base of 10 (e.g. log (10) = 2) and log (2) in order to obtain number of generations per number of days. Afterwards, one inverts it to obtain number of days per generation, which are the numbers used here to evaluate MG-63 cell's proliferation rate.

3.3: Results and Discussion:

3.3.1: Adhesion of MG-63 pre-osteoblast cells to different substrates

Focal adhesions are macromolecule assemblies that have integrin protein in their structure and (through signaling transduction) would link intracellular actin with extracellular substrates like extracellular matrices (ECM), usually for attachment. Focal adhesions have a dynamic assembly and dis-assembly relationship that plays an important role in cell migration. Initially, the multi-protein complex that makes up focal adhesions is unstable. But when certain components are presented to better stabilize it, focal adhesions would then be stationary with respect to ECM, and the cell would use that and their actin filaments as anchorage for attachment and movement. These focal

adhesions would anchor the ECM while moving towards the end of the cell's body before starting to dis-assemble. In other words, the stability and presence of focal adhesions would indicate cell's adherence to the ECM environment. Using the figures below, we investigated 1) if MG-63 cells seeded on each scaffolds would assemble robust focal adhesion and/or actin filaments and 2) on what that would mean in regards to their adherence to these different surfaces.

Figures 15, 17 and 18 below show three representative images each of IF staining of MG-63 cells seeded onto a coverslip, flat titanium (0.5 μm R_a value), and Plasmapore^{XP}'s (17.1 μm R_a value) surfaces, with nucleus (DAPI) in the blue channel, focal adhesion (Vinculin) in the green channel and actin (Phalloidin) in the red channel. "Channels" are filters that allow bright light's specific wavelength to pass through, e.g. "green channel" to allow 488 nm wavelength through and all others blocked. Figure 16 below shows two representative images of IF staining on MG-63 cells seeded onto PEEK (2.1 μm). Figure 19 represents the merged image comparisons between MG-63 cells on the coverslip, flat titanium, and Plasmapore^{XP}. All of these images are acquired with a 60x objective.

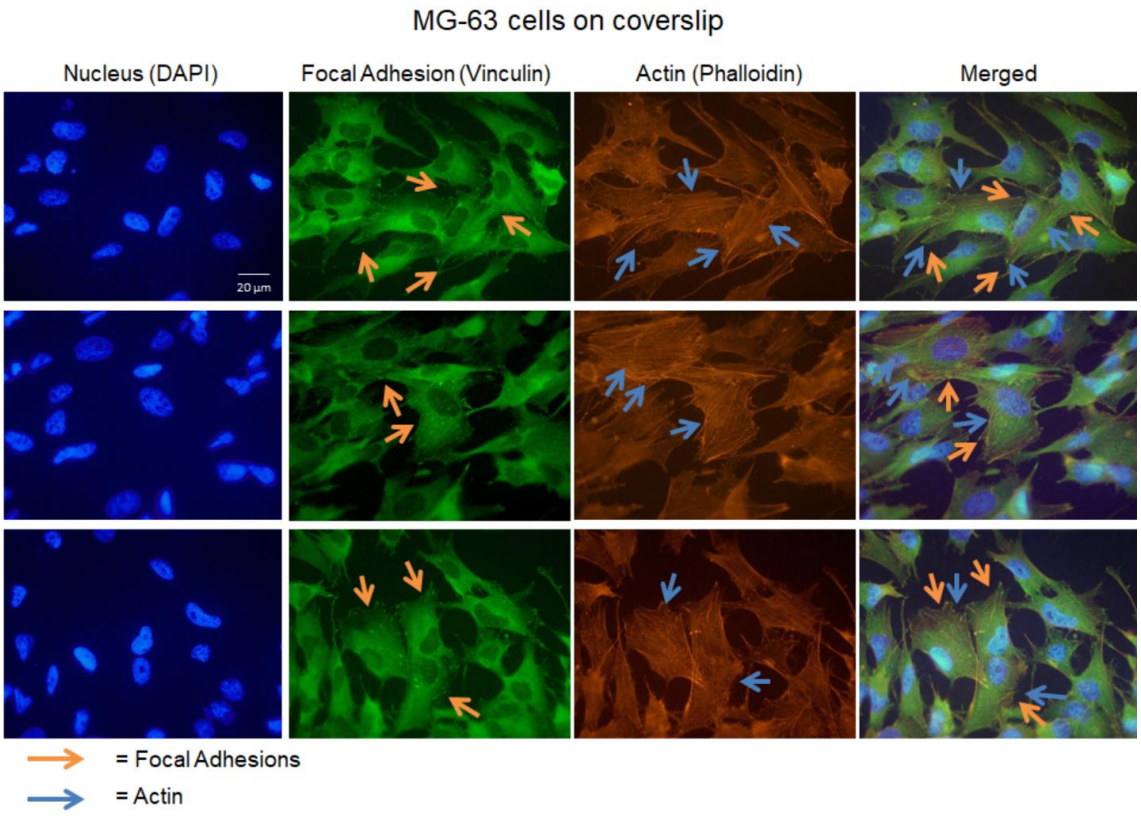

Figure 15: Human MG-63 osteoblast-like cells growing on glass coverslips. Three representative images of MG-63 cells growing on coverslips stained for cell nucleus (DAPI), focal adhesions (Vinculin), actin (Phalloidin), and all three stains merged. Cells were grown for 4 days before fixation and staining. Orange arrows indicate typical focal adhesions and blue arrows indicate actin stress fibers. Note the spread-out flat morphology of the cells. All images were acquired with an NA 1.4 oil immersion objective.

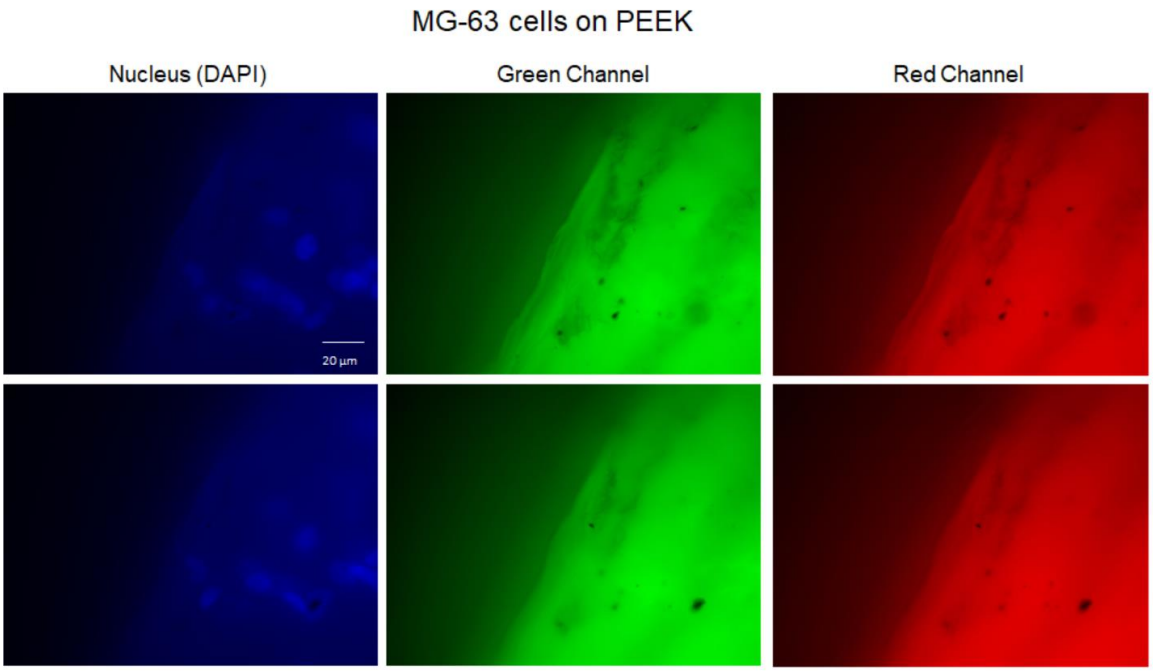

Figure 16: **MG-63 cells growing on PEEK.** MG-63 cells growing on PEEK's surface for 4 days, with Nucleus (DAPI), Anti-Vinculin (green) and Phalloidin (red) stains. The nuclei are visible, but not vinculin/focal adhesions or actin filaments due to PEEK's strong autofluorescent properties at these wavelengths. All images were acquired with an NA 1.4 oil immersion objective.

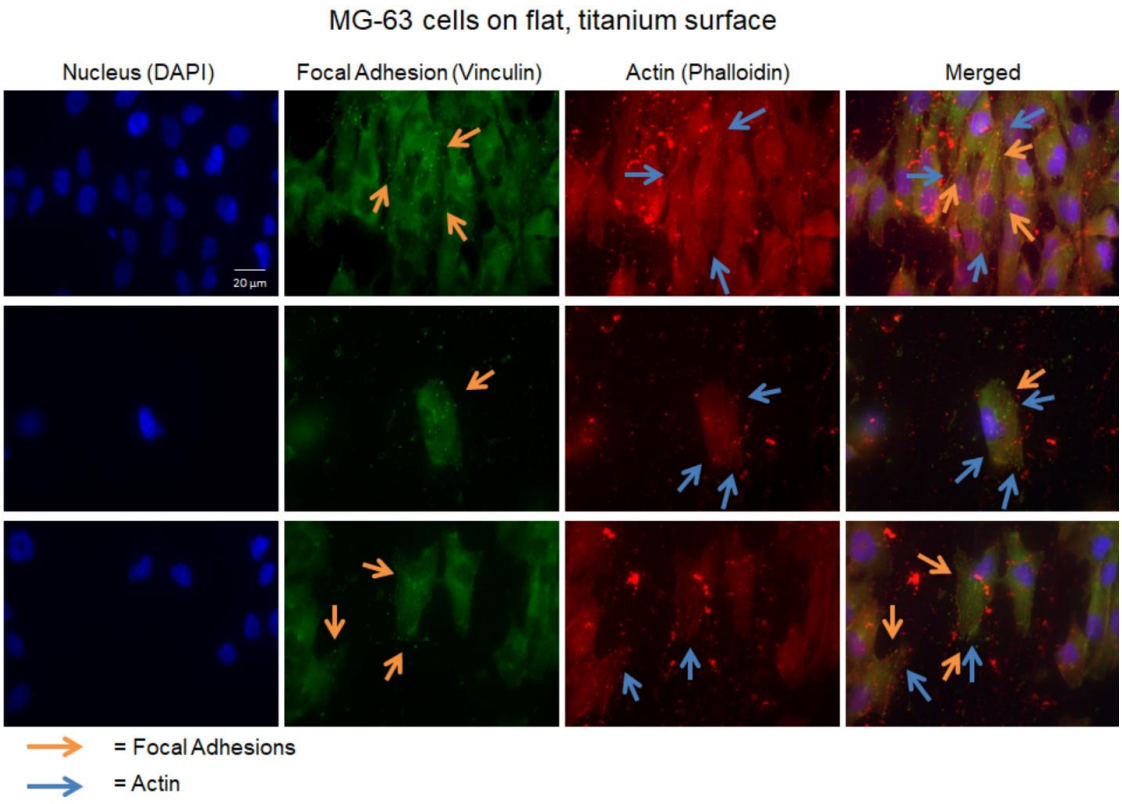

Figure 17: **MG-63 cells growing on a flat titanium surface.** Three representative images of MG-63 cells growing on a flat titanium surface stained for Nucleus (DAPI), Focal Adhesions (Vinculin), Actin (Phalloidin), and all three stains merged. Cells were grown for 4 days. Orange arrows indicate typical focal adhesions and blue arrows indicate actin stress fibers. Note the spread-out flat morphology of the cells. All images were acquired with an NA 1.4 oil immersion objective.

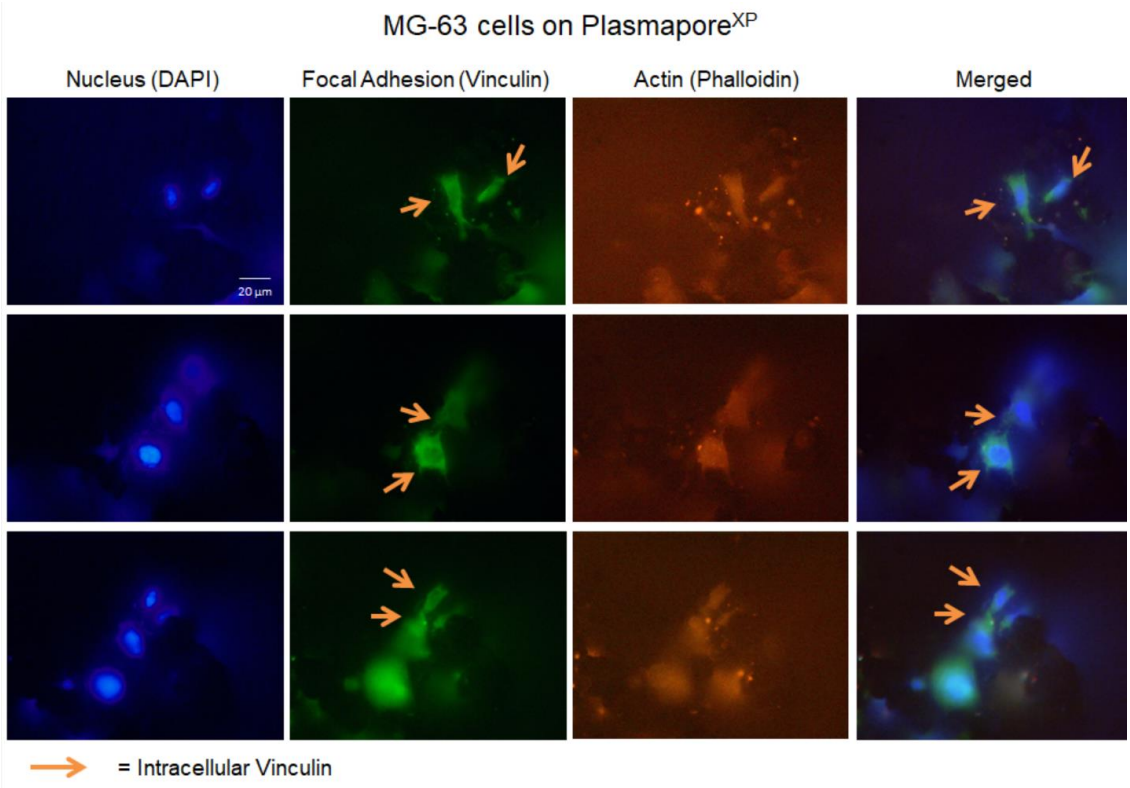

Figure 18: **MG-63 cells growing on Plasmapore^{XP}.** Three representative images of MG-63 cells growing on Plasmapore^{XP} stained for Nucleus (DAPI), Focal Adhesions (Vinculin), Actin (Phalloidin), and all three stains merged. Cells were grown for 4 days before fixation and staining. Orange arrows indicate typical focal adhesions and blue arrows indicate actin stress fibers. Note the smaller, more roundish morphology of the cells on this rough surface not showing distinct focal adhesions and actin stress fibers compared to the cells growing on smooth coverglass and titanium samples shown in Figures 15 and 17. All images were acquired with an NA 1.4 oil immersion objective.

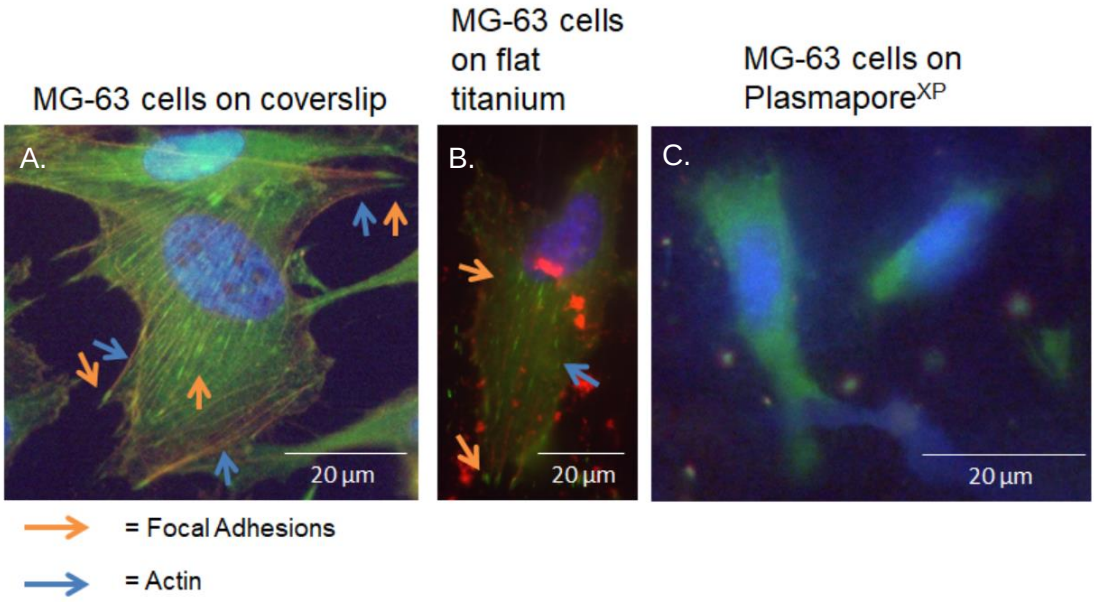

Figure 19: **High-magnification images of MG-63 cells growing on three different surfaces.** MG-63 cells growing on a coverslip, flat titanium surface and on Plasmapore^{XP}'s titanium surface for 4 days. Cropped, higher-magnified regions of images shown in Figures 15, 17, and 18 are shown to better visualize focal adhesions and actin stress fibers. Nuclei are stained with DAPI (blue).

Orange arrows in Figure 15 and 17 depict typical focal adhesions and blue arrows to indicate parallel organized actin stress fibers, while orange arrows in figure 18 depict vinculin localized in the cytoplasm. In Figure 16, MG-63 cell's nuclei are visible on PEEK's surface. But, vinculin/focal adhesions and actin filaments cannot be detected due to PEEK's strong autofluorescence properties at these wavelengths.

MG-63 cells in Figure 19, growing on coverslips (A) and on flat titanium (B), are both showing canonical focal adhesions, some of them at the end of actin filaments, while no typical focal adhesions are detectable in the cells growing on Plasmapore^{XP} (C). In addition, MG-63 cell's stress fibers are detectable in cells growing on coverslips and on flat, titanium while not detectable in cells growing on Plasmapore^{XP}. The presence of focal adhesions and actin stress fibers in cells growing on coverslips and flat titanium indicate that MG-63 cells strongly adhere to flat surfaces. Those cells on Plasmapore^{XP},

however, appear not to adhere well to the rough titanium surface. Moreover, cells on the coverslip and the flat, titanium surfaces spread out flat, while those on Plasmapore^{XP} exhibit a rounded, much less spread out morphology.

All of this information correlates with earlier investigations obtained in the Falk lab investigating MC3T3-E1 cell's growing on smooth and rough 45S5 Bioglass surfaces[32]. Figure 20 below shows representative IF images of MC3T3-E1 cells that were seeded onto a smooth (~0.1 μm R_a value) and a more rough (~1.2 μm R_a value) 45S5 Bioglass surface, with vinculin (focal adhesions) shown in red and phalloidin (actin stress fibers) in the green[32]. The purpose for these images is to compare Jain (2009)'s MC3T3-E1's morphology on Figure 20 with our MG-63's on smooth and rough surfaces (Figures 17-19).

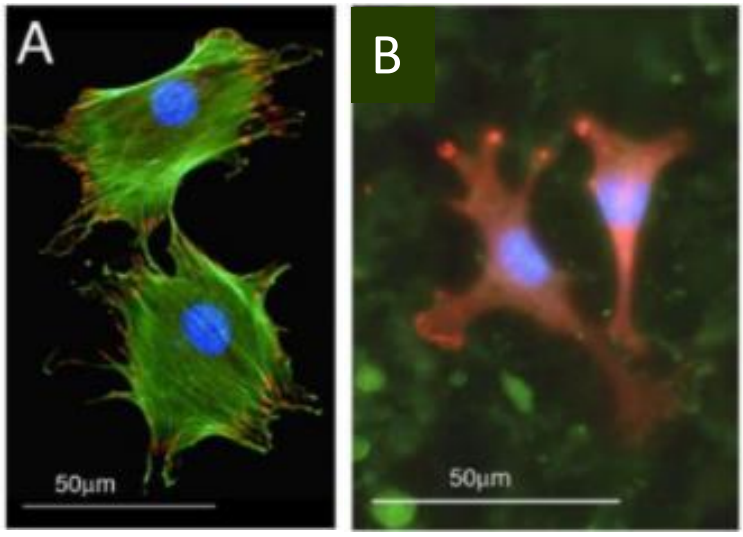

Figure 20: **MC3T3-E1 cells growing on 45S5 Bioglass surfaces.** Mouse MC3T3-E1 pre-osteoblast cells growing on smooth (A) and rough (C) 45S5 Bioglass surfaces for 12-24 hours. Actin is stained green, vinculin (focal adhesions) red, and cell nuclei are stained blue with DAPI[32]. Images are shown for comparison of morphology, and the formation of focal adhesions and stress fibers on another substrate with comparable smooth and rough surfaces.

MC3T3-E1 cells shown in Figure 20A exhibit focal adhesions preferentially in the cell's periphery and no defined focal adhesions in cells shown in Figure 20B, which indicates MC3T3-E1's stronger adhesion towards smoother 45S5 Bioglass surfaces than to rougher ones. In addition, MC3T3-E1 cells in Figure 20A show robust actin stress fibers while they are absent in MC3T3-E1 cells in Figure 20B, which would also indicate a reduced cell adhesion on rough 45S5 Bioglass surfaces. Moreover, the cells on the smooth surfaces spread out more, while cells on rough surfaces appear to spread out less. When comparing MG-63 cells on titanium's surface (Figures 19B and 19C) with MC3T3-E1 cells on 45S5 Bioglass (Figure 20A and 20B), cells on smooth/flat surfaces exhibit pronounced focal adhesions and actin stress fibers while cells on rough surfaces do not. In addition, cells spread out more on smooth/flat surfaces than on rougher ones. Both of these comparisons demonstrate how surface topology affects osteoblast behavior, and suggest that bone cells adhere better on smoother, flatter surfaces than on rougher ones.

One observation that is different between these two rough surfaces is that MG-63 cell's size appeared smaller when interacting with Plasmapore^{XP}'s surface while MC3T3-E1's size did not change when interacting with rough 45S5 Bioglass's surface. However, this observation should be investigated further.

It should be mentioned here that these studies were performed with osteoblasts only and no other bone-specific cell types or factors were present. When bone tissue adheres to an implant *in situ*, interactions are not limited to the bone tissue itself but also involve blood, lymph fluid, hormones and signaling proteins such as bone morphogenetic proteins (BMP) and transforming growth factor-beta (TGF-β) signaling proteins. Angiogenesis also plays an important role. Indeed, prior studies show that angiogenesis plays a vital role in bone repair[4]. Our *in vitro* studies are bone-forming cell-

type only “tissue” responses when initially interacting with various topological surfaces. This is part of osseointegration’s initial stage. During actual implantation, osteoblast cells spread out and directly contact the implant (adhesion and proliferation in *in vitro* terms) [33]. Once direct contact is established, osteoblast cells secrete calcified bone matrix materials such as hydroxyapatite (HA), collagen, and osteocalcin that surround them and stimulate osteoblast precursors to differentiate into mature osteoblasts and finally osteocytes, which are more mature bone cells and are the most abundant cell type in fully developed bone[34-36]. Osteocytes play a major role in mechanosensing (“feeling” the environment), regulating mineralization such as bone matrix or hydroxyapatite (HA), and controlling osteoblast and osteoclast’s activities, giving osteocytes a larger control over bone remodeling (the final steps of healing). Indeed, many studies show how high titanium surface roughness increases bone ingrowth and osseointegration towards their implants, which are vital for bone-implant interfacial strength and thus long-term stability[3,5,8,17-19,22-25]. Since these bone tissues have other biological components in addition to bone cells anchored to each other, it can be important to consider how blood, signaling molecules, and angiogenesis influence bone cell’s behavior, e.g. as in our studies, rough surfaces appear to reduce osteoblast attachment. It would be interesting to investigate how bone cells growing on TC Plastic or titanium, smooth and rough, would behave if a more complex, more bone-tissue like composition of cells and factors would be investigated.

3.3.2: Proliferation rate of MG-63 cells proliferating on the different scaffolds

Figures 21 and 22 show representative images of Live/Dead stained cells, as well as resulting linear and semi-logarithmic growth curves. All cells were imaged with a 20x objective.

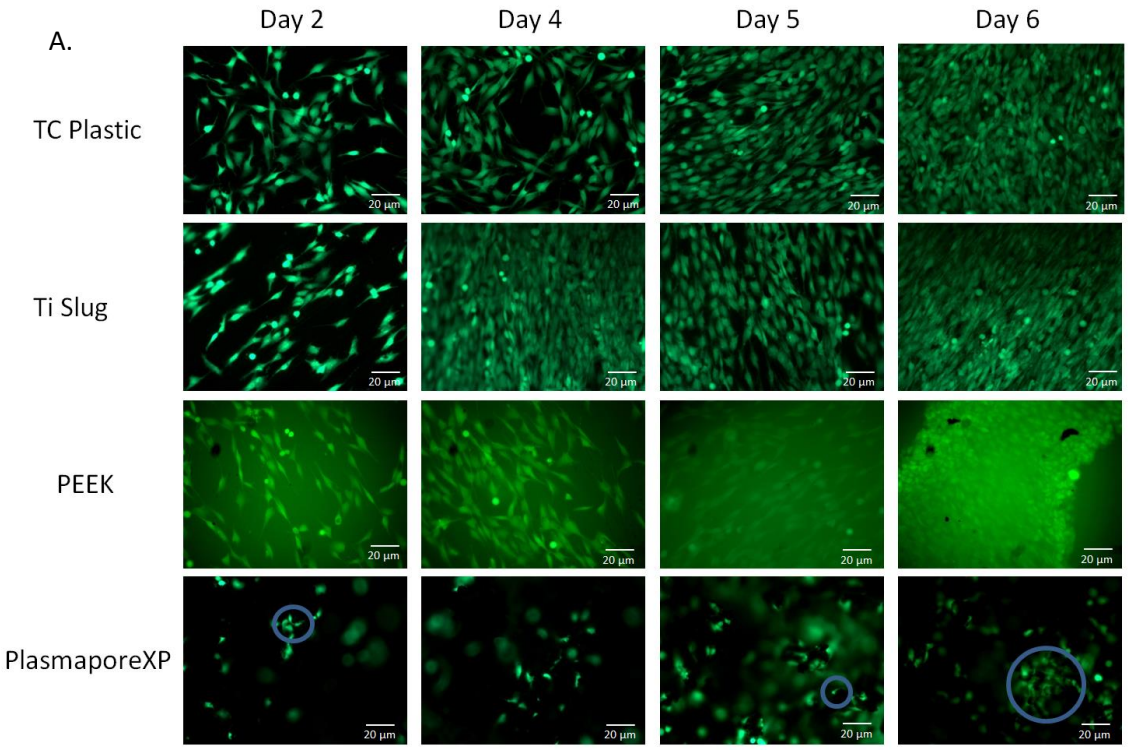

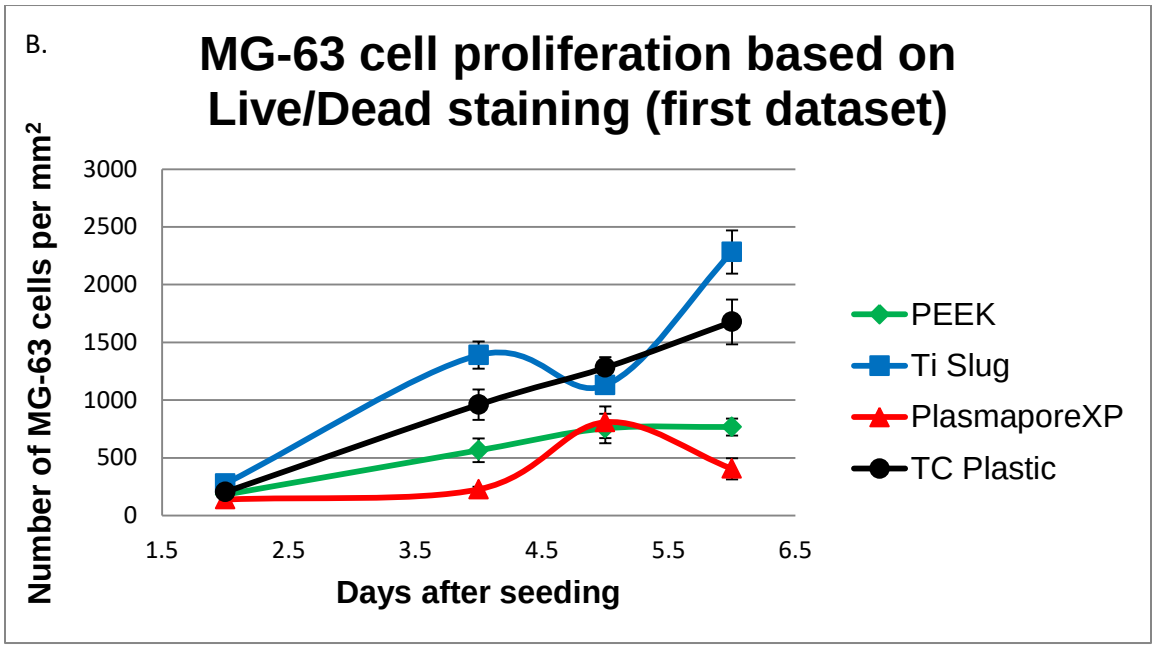

(Figure legend on following page)

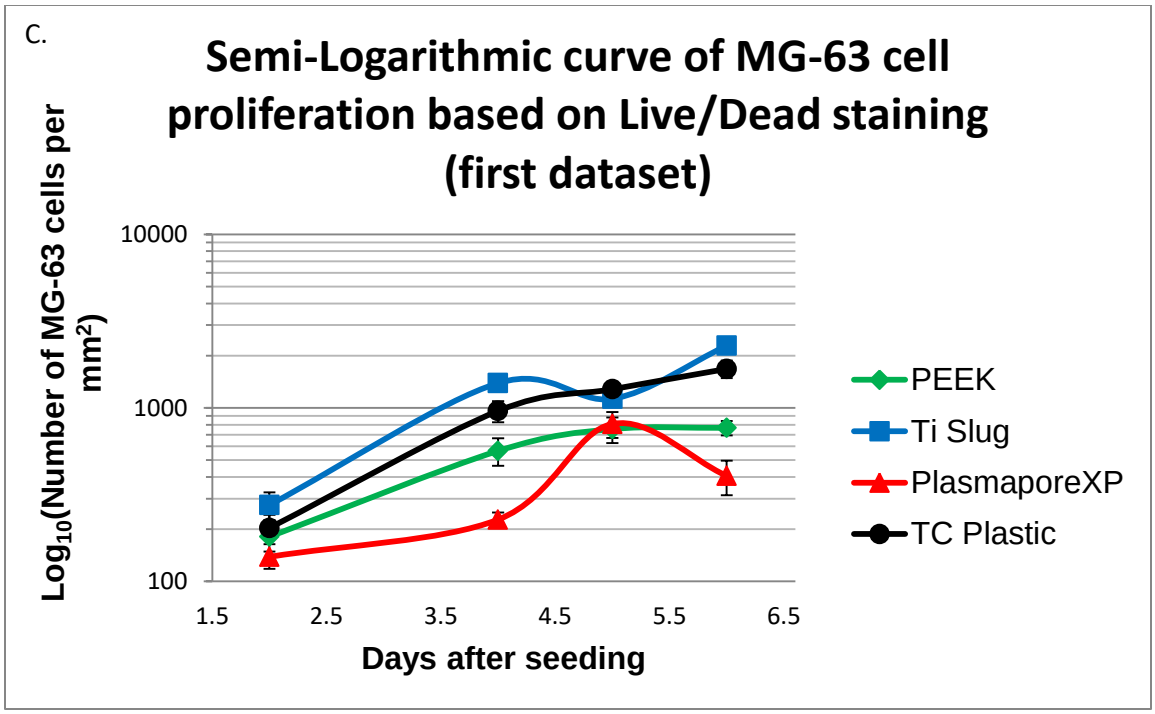

Figure 21: (**pg. 42-43**) **Example of calcein ("Live") staining of MG-63 cells on 4 different surfaces.** Images of calcein ("Live") staining of MG-63 cells grown on each surface imaged at indicated incubation times (a), representative linear proliferation curve (b), and the semi-logarithmic (c). 100 cells/mm^2 were seeded. Blue circles in (a.) represent MG-63 cells with rounded, off-shaped and smaller morphologies. Ethidium homodimer-1 ("Dead") staining is not shown since we are interested in viable cell's proliferation rate.

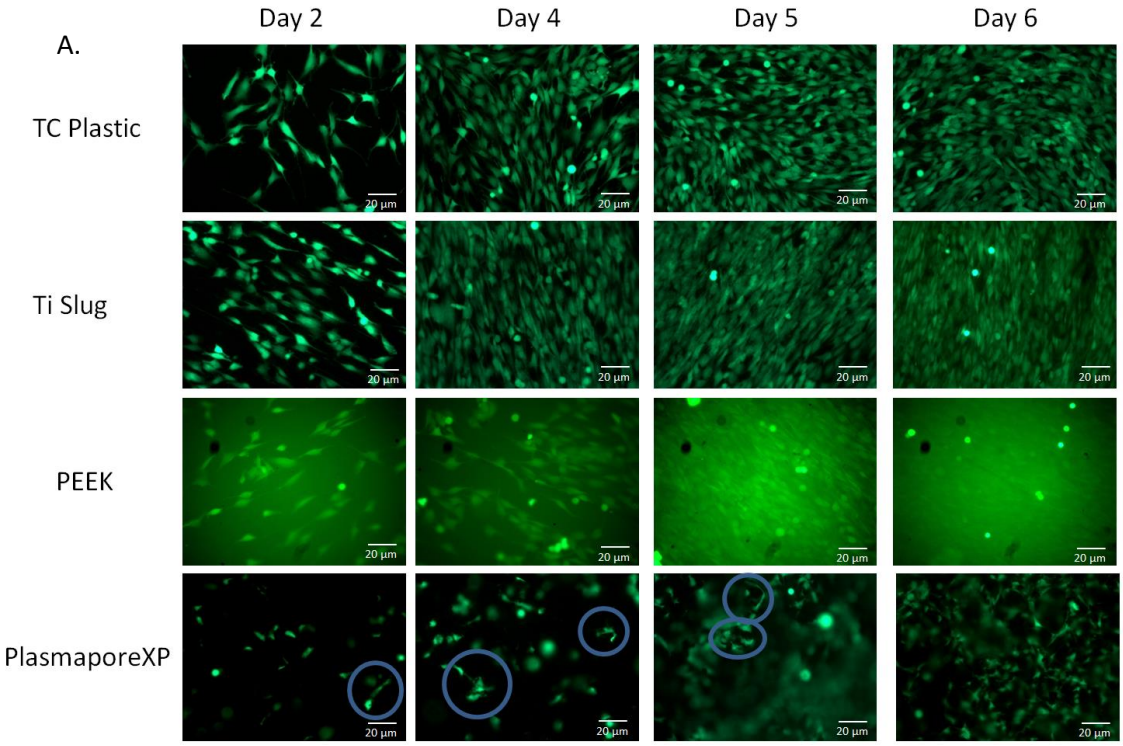

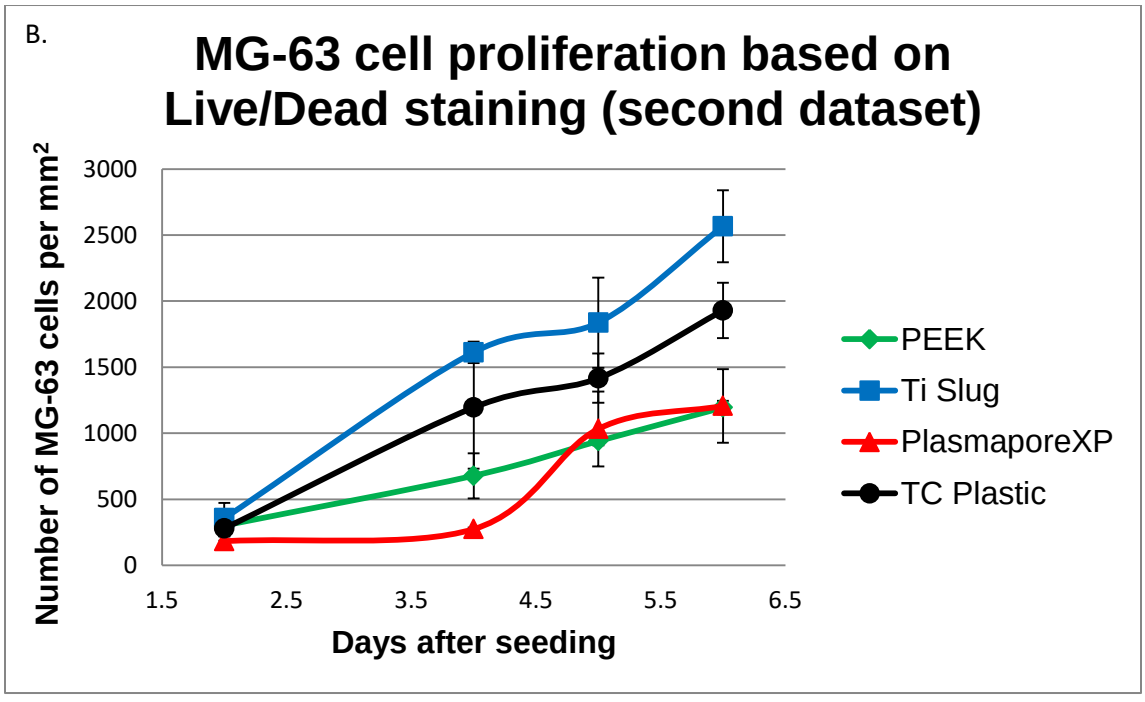

(Figure legend on following page)

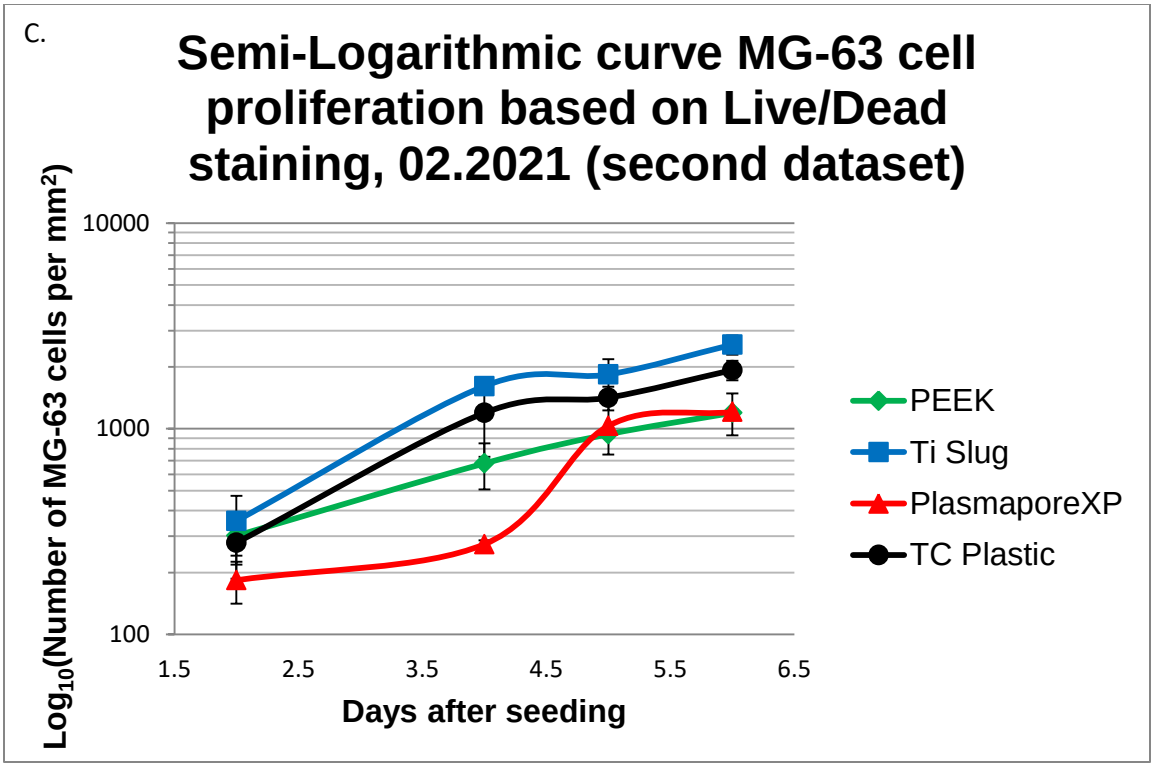

Figure 22: (**pg. 44-45**) **Another example of calcein ("Live") staining of MG-63 cells on 4 different surfaces.** Images of calcein ("Live") staining of MG-63 cells grown on each surface imaged at indicated incubation times (a), representative linear proliferation curve (b), and the semi-logarithmic (c). 100 cells/mm^2 were seeded. Blue circles in (a.) represent MG-63 cells with rounded, off-shaped and smaller morphologies. Ethidium homodimer-1 ("Dead") staining is not shown since we are interested in viable cell's proliferation rate.

The collage of images in Figure 21A and 22A represent MG-63 cells stained by calcein-AM. Images of MG-63 cells stained by ethidium homodimer-1 ("Dead") are not shown because our proliferation rate evaluation is based on viable cell's proliferation. In addition, "Dead" cell counting cannot be compared to WST-1 assay, which will be discussed in Figure 23 below. On TC Plastic and flat titanium ("Ti Slug"), one can visually appreciate their numbers increase over time. Note that autofluorescence of PEEK is visible and blurs image clarity. However, its intensity is not high enough to overwhelm the calcein staining. (PEEK's autofluorescence in fluorescence microscopic applications is common[37-39]). A peculiar and unexplained observation is that after 5-6

days of seeding on PEEK, the cells appear to have a weaker calcein-AM signal and seem photobleach at a faster rate. Reduced metabolic activity at these later time points (correlating with a potentially slower proliferation rate) could explain this observation, however, will need further examination. Another interesting observation that correlates with previously described immunofluorescence-based observations relates to the morphology of MG-63 cells growing on Plasmapore^{XP}. Cells growing on flat titanium, TC Plastic, or PEEK usually exhibit an elongated, epithelioid morphology (Figures 21A, 22A, top three rows), while cells on Plasmapore^{XP}, appear more rounded, off-shaped and smaller. Some of these morphologies are circled (Figure 21A, 22A, bottom row). IF analyses of these cells shown in Figure 19 indicate that MG-63 cells attached to Plasmapore^{XP} do not show robust focal adhesions or actin stress fibers, which correlate with their morphology shown here. Overall, cells interacting with any of the smooth surfaces (TC Plastic, flat titanium, or PEEK) share the same morphologies while cells on the rougher surfaces do not share that morphology. Thus even the same material (titanium), surface topology can affect cell adhesion (Figures 17-19) and their morphology (Figure 21A and 22A) based on how they “adjust” to these surfaces.

In Figures 21B/C, and 22B/C, MG-63 cells are proliferating on all four samples, though not with the same rate. 100 cells/mm^2 were seeded in these experiments per sample. As shown in Figure 21, deduced growth curves indicate that in this experiment cells growing on top of a flat titanium surface exhibit a duplication time of 31.2 ± 4.8 hours, cells in tissue culture dish’s duplicated every 36.0 ± 7.2 hours, cells on PEEK duplicated every 45.6 ± 9.6 hours, and cells on Plasmapore^{XP} duplicated every 74.4 ± 26.4 hours. In the second experiment, as shown in Figure 22, cells on top of flat titanium exhibited a duplication time of 26.4± 2.4 hours, cells in tissue culture dishes duplicated every 31.2 ± 2.4 hours, cells on PEEK every 36.0 ± 4.8 hours, and on Plasmapore^{XP}

every 48.0 ± 14.4 hours. The average of both experiments indicates a duplication time of 28.8 ± 2.7 hours for flat titanium, 33.6 ± 3.8 hours for TC plastic, 40.8 ± 5.4 hours for PEEK, and 61.2 ± 15.1 hours for Plasmapore^{XP}. The decreasing cell numbers on Plasmapore^{XP} found after 5 days (Figure 21B/C, 22B/C) likely is an experimental error and could be an effect of the implants high porosity, allowing cells to proliferate inside the void pockets, however negatively affecting the Live/Dead staining and cell counting accuracy. This has been addressed further using cell counts based on enzymatic WST-1 assays which do not show such a proliferation dip (see below and Figure 23). The unexpected dip in cell growth between days 4-6 on flat titanium observed in both experiments again is considered an experimental error as WST-1-based growth experiment do not show reduced growth on these days post seeding (see below and Figure 23). Nevertheless, both figures and the duplication time calculations indicate that MG-63 cells proliferate faster on the surface of flat titanium or TC plastic compared to growing on the surface of PEEK, or Plasmapore^{XP}. Titanium's biocompatible property and the culture dish's charges and resulting high hydrophilicity (achieved by Nunclon Delta surface treatment[39]) are favorable, while PEEK has neither of these properties, resulting in cells proliferating faster on those two surfaces than on PEEK. Although Plasmapore^{XP} is also composed of titanium, its rough surface topology likely makes cell's adhesion more difficult (see Figures 17-19), resulting in a slower proliferation on Plasmapore^{XP}. Cheng and Aesculap has also shown reduced adhesion and proliferation of MG-63 cells growing on Ti-PEEK (complete Arcadius Plasmapore^{XP} implants) and on PEEK compared to TC plastic, on day 1 and 7 after seeding using WST-1 based cell proliferation assays[23].

Compared to Live/Dead staining, WST-1 assays indirectly measure cell density based on enzymatic activity of live cells.

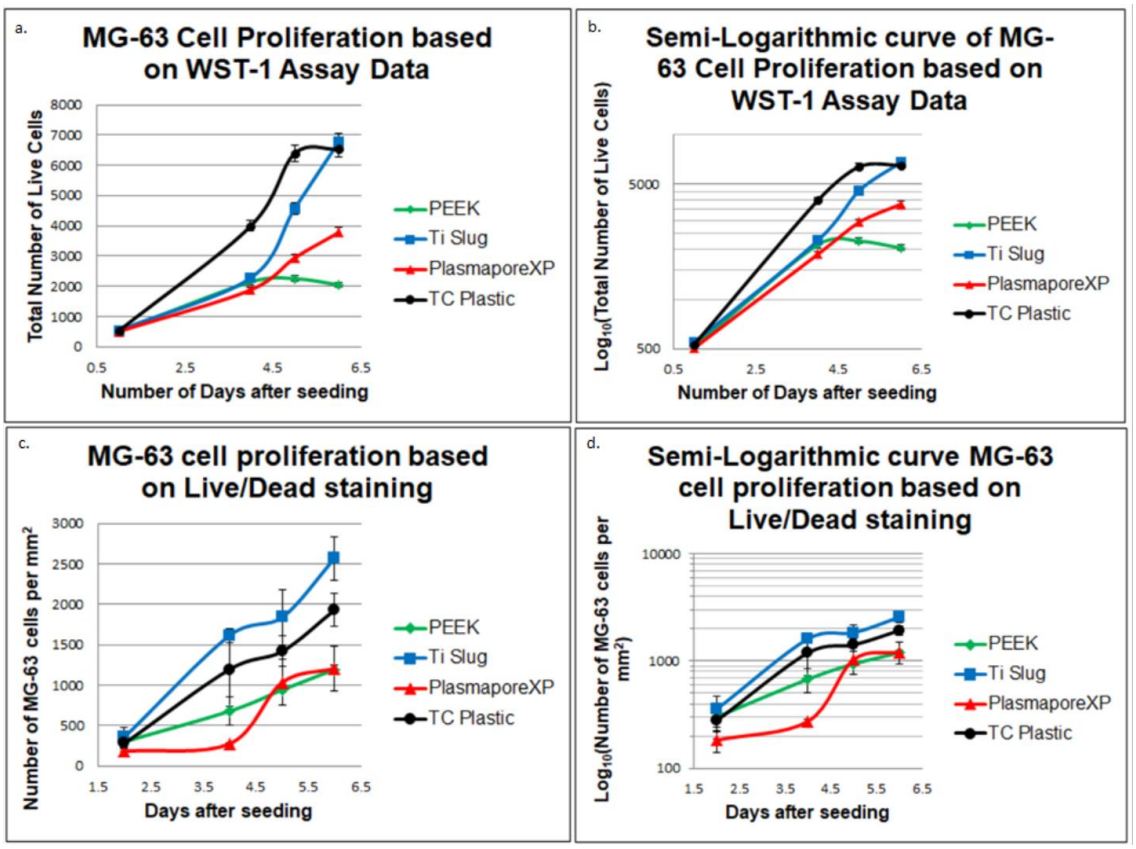

Figure 23: **Comparison of linear and semi-logarithmic WST-1 and Live/Dead staining MG-63 cell proliferation curves.** MG-63 cell proliferation based on Live/Dead staining (in a and c), and WST-1 assay (in b and d) (a and c, linear; b and d, semi-logarithmic representation). Live/Dead staining directly shows cells while WST-1 assay indirectly measures cell density by enzymatic activity that is exhibited by viable cells.

Figure 23 above shows a comparison of cell growth based on Live/Dead staining (Figure 22) and WST-1 assays. When calculating cell duplication rates based on WST-1 enzyme assays we found that cells on top of flat titanium duplicated every 33.6 ± 1.9 hours, cells on tissue culture plastic duplicated every 28.8 ± 4.8, cells on PEEK duplicated every 45.6 ± 12.0 hours, and on Plasmapore^{XP} every 38.4 ± 1.9 hours. Again, as observed with Live/Dead staining described above, MG-63 cells proliferate faster on the surface of flat titanium or tissue culture dishes than on PEEK or Plasmapore^{XP}. Interestingly, duplication time for MG-63 cells growing on Plasmapore^{XP} was determined to be 61.2 ±

15.1 hours based on Live/Dead staining, and 38.4 ± 1.9 hours based on WST-1 assay. The duplication time and their standard deviations are different from each other. This discrepancy could be due to the technique of Live/Dead staining and WST-1 assay. As stated before, Live/Dead staining directly measure cell density based on cell counts in the images, while WST-1 assays indirectly measure cell density based on enzymatic activity of live cells. From Plasmapore^{XP}'s cross-section SEM in Figure 13, its porosity would allow cells to seep into these pockets, affecting the cell counts in the images when performing Live/Dead staining experiment. Since WST-1 absorbance readings do not require human eye visions, the enzymatic reading's cell counting would include cells on the surface and deep into Plasmapore^{XP}'s pockets.

Why might osteoblasts proliferate slower on rougher compared to smoother surfaces? As described in Chapter 1, bone cells either proliferate or differentiate, not both; in fact, an inverse relationship between these two fates is well described[39]. If an osteoblast bone cell differentiates while adhering onto a rough surface, its proliferation rate will likely decrease. Prior studies were showing how rougher surfaces increase osseointegration between bone tissues and implants over longer periods of time (weeks to months) [3, 5, 17-19]. In addition, one of these studies specifically indicated that after 7 days, bone cells exhibited a higher differentiation rate on rougher surfaces than on smoother ones[23]. It is possible that bone tissue when first interacting with the implant's rough surface, faces difficulties attaching because pre-osteoblasts are more accustomed to adhering to flatter surfaces. So as time passes, the immature bone cells' morphology may change and they differentiate in order to better adhere to the rougher implant surfaces, transforming into fully mature bone cell. This adaptation and differentiation process requires time, which may explain why three months is necessary for bone tissue to fully adhere to implants with rougher titanium surfaces.

Chapter 4: Conclusions and Future Directions

4.1: Conclusions

4.1.1: Material characterization of the three investigated materials

The elemental composition analysis from Energy Dispersive Spectroscopy (EDS) shows that both the flat titanium and Plasmapore^{XP} implant's surfaces contain primarily titanium. However, Plasmapore^{XP} shows a high concentration of nitrogen, possibly due to contaminations encountered during the fabrication process. High concentration of carbon was also detected, however that could be a result of an interference from PEEK or contaminations encountered during EDS analysis. This contamination is important to note when comparing bone cell's behavior towards flat and rough titanium surfaces. Both Scanning Electron Microscopy (SEM) and the Profilometer measurements indicate that Plasmapore^{XP} is much rougher than flat titanium. The R_a values measured with the profilometer for the two materials are 17.1 ± 1.2 μm, and 0.5 ± 0.06 μm, respectively. However, the measured value for Plasmapore^{XP} is significantly underestimated because the profilometer needle tip cannot fully probe Plasmapore^{XP}'s tortuous porosity. The cross-sectional SEM image shown in Figure 13 gives more accurate, although not as quantitative, information about the implant's surface roughness. The R_a value for the PEEK component of the implant was determined as 2.1 ± 0.4 μm.

4.1.2: Biological responses related to cellular attachment

Immunofluorescence (IF) and Live/Dead staining show that when cells interact with flat surfaces such as culture dishes, flat titanium, or PEEK, they spread out forming lamellipodial extensions. By comparison, on Plasmapore^{XP} the cells morphology is not as flat or spread out as on smooth titanium or tissue culture plastic surfaces. As clearly

visible in IF staining images shown in Figures 17-19, human MG-63 osteoblast-like bone cells adhering to flat surfaces show typical, more robust focal adhesions and actin stress fibers compared to adhering to Plasmapore^{XP}'s rough, porous surface. In comparison, mouse MC3T3-E1 pre-osteoblast cells also form robust focal adhesions and actin stress fibers on smooth 45S5 Bioglass surfaces but not on rough glass (R_a ~ 1.2 µm) of the same composition[32]. Based on these findings, we can conclude that bone cells appear to adhere stronger to flatter surfaces than to rougher and more porous surfaces.

4.1.3: Adhesion and cell proliferation to smooth and rough surfaces

The observations using MG-63 cells show that they proliferate faster in tissue culture dishes or on flat titanium than on PEEK or Plasmapore^{XP}. Based on my IF staining, bone cells appear to adhere stronger to flatter surfaces than onto rougher ones. These differences could explain why I observed a slower proliferation rate on Plasmapore^{XP} than on the other two materials investigated also in this study. PEEK is not a biocompatible or favorable cell adhesion material, thus adhesion to its surface was not expected. Cheng and Aesculap also showed similar adhesion and proliferation of MG-63 cells on PEEK vs. Ti-PEEK (the material of Plasmapore^{XP}) surfaces. Also, their total cell count after 3 hours (adhesion) and 7-10 days (proliferation) of seeding are lower than those on tissue culture dishes[23]. Overall, rougher surfaces create a bigger obstacle for bone cells to adhere to their surfaces, which would negatively impact their proliferation rate over short periods of time (hours to days).

4.2: Future Directions

4.2.1: Investigate the source of extra carbon and nitrogen in our Plasmapore^{XP} samples

As discussed in Chapter 2, the EDS spectroscopy identified some unexpected elements in addition to titanium: nitrogen and carbon. Since these extra elements are not

there by design, their presence needs to be confirmed and their source needs to be established. Since Plasmapore^{XP} was designed by Aesculap, further knowledge on the manufacturing and processing process would be beneficial to better be able to determine where these contaminations might be derived from.

4.2.2: Coating of Plasmapore^{XP} to modulate cell/scaffold interactions

Bone cells adhere better to culture dishes because these dishes were treated with Nunclon Delta, which makes them charged and thus more hydrophilic and thus promotes strong adhesion to these surfaces[40]. Coating an implant such as Plasmapore^{XP} surface to make it more hydrophilic/charged would potentially improve bone cell adhesion. One study showed an increase in titanium implant hydrophilicity and wettability when incubated with an isotonic solution of 0.9% sodium chloride solution[41]. When inserting implants into the rabbit's tibias leg, the one with that incubation showed better osseointegration than the one without incubation. Thus, it might be possible to incubate Plasmapore^{XP} with a solution, such as 0.9% isotonic sodium chloride solution, to increase implant hydrophilicity and osseointegration.

A similar approach could be to coat Plasmapore^{XP} surfaces with a bioactive glass such as 45S5 Bioglass or tailored amorphous multi-porous (TAMP) calcium silicate glass developed at Lehigh University.

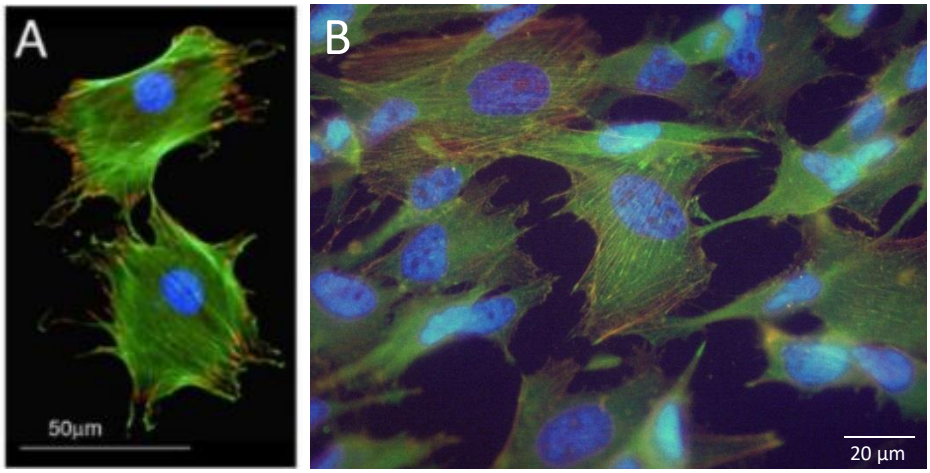

Figure 24: **Comparison of MC3T3-E1 and MG-63 bone cells growing on smooth surfaces.** (A) MC3T3-E1 cells growing on a smooth 45S5 Bioglass surface (R_a ~0.1 µm) with actin (phalloidin) labeled green and focal adhesions (vinculin) labeled red.[32] (B) MG-63 cells growing on a coverslip with actin (phallodin) labeled red and focal adhesions (vinculin) labeled green. Nuclei are labeled with DAPI (blue).

Figure 24 above shows IF staining of MC3T3-E1 cells growing on a smooth 45S5 Bioglass surface[32] (A) and MG-63 cells growing on a glass coverslip (B). Both cell types in these images show typical focal adhesions and actin stress fibers when MC3T3-E1 and MG-63 cells are interacting with smooth 45S5 Bioglass and coverslip surfaces, respectively. In addition, focal adhesions are localized preferentially to the cell's periphery. Importantly, bioglass exhibits a higher bioactivity than titanium, suggesting that bioglass stimulates bone regeneration better than titanium. For *in vitro*, that would indicate a higher proliferation rate on bioglass-titanium composition than titanium alone; a hypothesis that is confirmed by prior studies[42-43]. Moreover, studies have shown that bioactive glass can increase bone cell's attachment to these surfaces, in addition to proliferation/regeneration[43].

The original bioactive glass composition called 45S5 Bioglass was made by L.L. Hench; he showed how it naturally bonds to bone[44-45]. In addition, bioactive glass has a

better chance of integrating with human bone tissue than metal implants do[46]. It was also found that one can coat metal implants with bioactive glass compositions. The coating techniques commonly included enameling or sol-gel[46-47]. Both of these techniques involve heating ceramics, like glass here, to allow them to fuse with the metal. However, sol-gel also requires high temperature in post-treatment (after first heating) in order to solidify this glass's fixation[46]. Sol-gel coating would be our coating choice because that procedure is established at Lehigh University and it allows for a simpler control of glass porosity.

There are also additional techniques that can improve bioactive glass's biological performance more than the original 45S5 Bioglass. Drs. Jain and Falk published numerous articles to show how nanoporosity improves bioactive glass's biological performances; and even created bioactive glasses with intrinsic nanoporosity termed TAMP[48-50]. Their *in vitro* studies showed that MC3T3-E1 bone cells attach stronger to bioactive glass that has a smaller nanopore size (size compared to what other size, give both sizes here), which indicates that TAMP is bioactive and that its surface topology plays an important role in bone cell's behavior[48]. These nanopores have pore sizes from 3-17 nm, which is substantially smaller than Plasmapore^{XP}'s (50-100 µm), thus surface topology is still preserved here. Also, their *in vivo* studies showed that the nanopores of bioactive glasses promote bone cell colonization and penetration into these scaffolds, suggesting a high potential for increased osseointegration when TAMP is coated onto Plasmapore^{XP} metal implants. An important step in the use of these coatings would be to incubate bioactive glass in simulated bodily fluid (SBF) to stabilize it against any toxicity against cells, which can occur at the beginning[51].

Another, alternative coating option of Plasmapore^{XP} could deploy extracellular matrix (ECM) or bone morphogenic proteins (BMPs), or relevant adhesion peptides

including RGD amino acid sequence motifs. It is known that ECM proteins such as collagen or fibronectin stimulate bone regeneration and osseointegration *in vivo*[52]. Coating procedures could be done as described by Stadlinger to coat titanium implants with collagen, collagen/chondroitin sulfate (cartilage's structural component), and collagen/chondroitin sulfate/BMP-4 [5254].

4.2.3: Investigate cell response related to differentiation

Cheng and Aesculap evaluated bone cell's behavior towards Plasmapore^{XP} regarding adhesion, proliferation and differentiation, whereas this study focused on the first two stages of cell response. [23] Schwartz showed that increasing pedicle screw's microscale roughness increased osteoblast differentiation and ECM production, and stimulates stronger bone formation and osseointegration[54]. Thus, an important next step should involve expanding the present study to also include cell differentiation. The mechanism behind bioactive glass's enhanced biological performance is that it stimulates collagen type 1, alkaline phosphatase (ALP) and osteocalcin production, all differentiation markers which are important for bone regeneration[55]. Cheng and Aesculap used ALP/BCA (bicinchoninic acid) assays, BMP (bone morphogenic protein) assays, and RT-PCR (reverse transcription – polymerase chain reaction) based gene expression to analyze MG-63 cell's differentiation rate towards Ti-PEEK, PEEK, and TC plastic samples[23]. Though ALP is a differentiation marker, BCA measures total protein; this assay is important to verify if increasing or decreasing ALP expression relates to differentiation rate or total protein production. ALP can for example be determined with an AnaSpec SensoLyte pNPP ALP assay kit (AnaSpec, Inc., Fremont, CA, USA) that can be purchased from Pierce Biotechnology (Rockford, IL, USA). BMP is a growth factor, particularly to stimulate bone and cartilage formation. Overall, increasing bone

cell differentiation is likely to increase bone regeneration, repair, and bone-implant interfacial strength.

4.2.4: Detecting additional focal adhesion components related to sensing the cellular environment

In our study, we use nuclei (DAPI), vinculin (green channel) and actin/phalloidin (red channel) stains to evaluate cellular attachment. Another possibility would be to stain for active, phosphorylated-focal adhesion kinase (phospho-FAK). IF staining of MG-63 cells growing on glass coverslips including cell nuclei (DAPI), actin/phalloidin (green) and phospho-FAK (red) is shown in Figure 25.

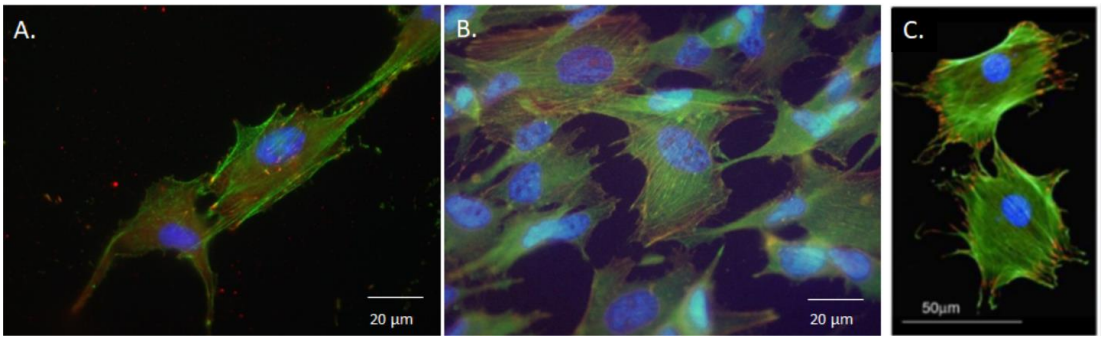

Figure 25: Comparison of phospho-FAK (focal adhesion kinase) with vinculin (another focal adhesion component) staining. IF staining of (A) MG-63 cells growing on a glass coverslip stained for actin (Phalloidin, green channel) and phospho-FAK (Rabbit antibody, Catalog # 44-624G red channel), (B) MG-63 cells growing on a coverslip stained for actin (Phalloidin, red channel) and anti-Vinculin (Mouse antibody, green channel), and (C) MC3T3-E1 cells growing on smooth 45S5 Bioglass stained for actin (Phalloidin, green channel) and anti-vinculin (Mouse antibody, red channel)[32].

Phospho-FAK staining indicates whether a focal adhesion is active as it only stains activated focal adhesions. An increase in FAK's phosphorylation at serine 397 occurs when integrins are attached to fibronectin (an ECM protein). In other words, increased

FAK phosphorylation indicates that more integrins bind to fibronectin or other ECM proteins.

In addition, staining cells with anti-paxillin antibodies is another informative approach. Yirka et al. proposed that the focal adhesion protein paxillin plays an important role in sensing surrounding environment of a cell and aids cells to make anchoring choices when navigating in an environment[57]. In addition, paxillin's C-terminal region is involved in binding to focal adhesions, which could help to better evaluate cellular attachment[58].

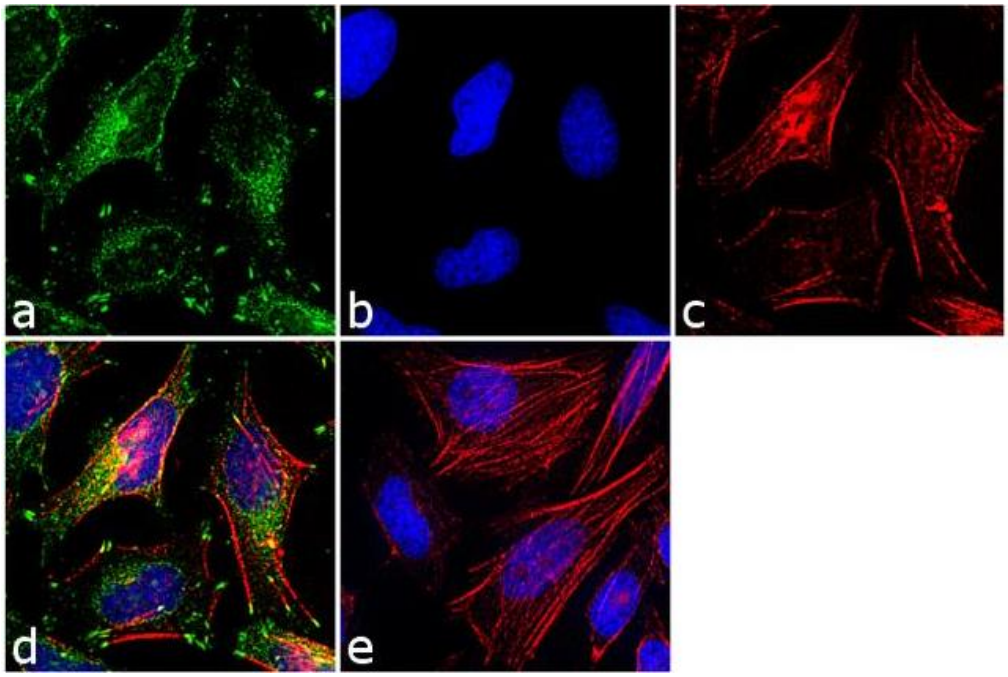

Figure 26: **IF staining of paxillin in HeLa cells.** HeLa cells were grown on glass coverslips and processed for IF. The focal adhesion protein, paxillin was detected with mouse anti-paxillin antibody (ThermoFisher Scientific, Catalog Number: MA5-13356) and detected with goat anti-mouse (IgG (H+L) Superclonal™ secondary antibody) Alexa Fluor® 488 conjugate (a), cell nuclei were stained with DAPI (b), and F-actin was decorated with "Rhodamine Phalloidin" (c). Merged channels (a to c) are shown in (d).The image in (e) is the no primary antibody control, to demonstrate that the stain detected in (a) is specific for paxillin.

Thus, staining with both antibodies directed against paxillin and phospho-FAK would identify focal adhesions that function in attaching and mechano-sensing the environment at the same time.

4.2.5: Investigating osteoblasts attached to Plasmapore^{XP} with SEM

In this study, osteoblasts attaching to PlasmaporeXP as well as other surfaces were examined using immunofluorescence-based light microscopic techniques as well as enzyme-based (WST-1) assays. While these assays provided valuable information on the attachment and proliferation their resolution is limited. For example, Kowal et al. investigated interaction of MC3T3-E1 pre-osteoblasts with TAMP scaffolds using both, IF and SEM analyses[49]. Thus, similarly investigating MG-63 cells or MC3T3-E1 cells interacting with Plasmapore^{XP} would likely further add valuable, high-resolution morphological information.

References:

1. OpenStax College, *Anatomy and Physiology*. Retrieved from OpenStax CNX: http://cnx.org/contents/14fb4ad7-39a1-4eee-ab6e-3ef2482e3e22@11.1

2. Sumita, M., Hanawa, T. (2003). 9.04 - Failure Processes in Biometallic Materials. (R. O. In I. Milne, Ed.) *Comprehensive Structural Integrity, 9*, 131-167.

3. Mavrogenis, A. F., Dimitriou, R. (2009). Biology of implant osseointegration. *Journal of musculoskeletal & neuronal interactions, 9*(2), 61–71.

4. Saran, U., Gemini Piperni, S., & Chatterjee, S. (2014). Role of angiogenesis in bone repair. *Archives of biochemistry and biophysics*, *561*, 109–117. https://doi.org/10.1016/j.abb.2014.07.006

5. Abraham C. M. (2014). A brief historical perspective on dental implants, their surface coatings and treatments. *The open dentistry journal, 8*, 50–55.

6. Saini, M., Singh, Y., Arora, P., Arora, V., & Jain, K. (2015). Implant biomaterials: A comprehensive review. *World journal of clinical cases*, *3*(1), 52–57. https://doi.org/10.12998/wjcc.v3.i1.52

7. *Corrosion Resistance of Titanium.* (2011, 07). Retrieved from United States Nuclear Regulatory Commission: https://www.nrc.gov/docs/ML9932/ML993210187.pdf

8. Parithimarkalaignan, S., & Padmanabhan, T. V. (2013). Osseointegration: an update. *Journal of Indian Prosthodontic Society*, *13*(1), 2–6. https://doi.org/10.1007/s13191-013-0252-z

9. *Fusion with Interbody Cages*. (2003). Retrieved from University of Maryland, Medical Center: https://www.umms.org/ummc/health-services/orthopedics/services/spine/patient-guides/fusion-interbody-cages

10. *Intervertebral Cages*. (n.d.). Retrieved from The B.A.C.K. Center: https://www.thebackcenter.net/intervertebral-cages.html

11. *Aesculap ArcadiusXP L.* (n.d.). Retrieved from DocPlayer: https://docplayer.net/47122457-Arcadius-xp-l-spinal-system-product-brochure-aesculap-spine.html

12. Krayenbühl, N., Schneider, C., Landolt, H., & Fandino, J. (2008). Use of an empty, Plasmapore-covered titanium cage for interbody fusion after anterior cervical microdiscectomy. *Journal of clinical neuroscience : official journal of the Neurosurgical Society of Australasia*, *15*(1), 11–17. https://doi.org/10.1016/j.jocn.2006.12.011

13. Butterman G. R. (2018). Anterior Cervical Discectomy and Fusion Outcomes over 10 Years: A Prospective Study. *Spine, 43*(3), 207–214.

14. Martin, C. T., D'Oro, A., Buser, Z., Youssef, J. A., Park, J. B., Meisel, H. J., Brodke, D. S., Wang, J. C., & Yoon, S. T. (2018). Trends and Costs of Anterior Cervical Discectomy and Fusion: a Comparison of Inpatient And Outpatient Procedures. *The Iowa orthopaedic journal*, *38*, 167–176.

15. Saifi, C., Fein, A. W., Cazzulino, A., Lehman, R. A., Phillips, F. M., An, H. S., & Riew, K. D. (2018). Trends in resource utilization and rate of cervical disc arthroplasty and anterior cervical discectomy and fusion throughout the United States from 2006 to 2013. *The spine journal: official journal of the North*

American Spine Society, *18*(6), 1022–1029. https://doi.org/10.1016/j.spinee.2017.10.072

16. Lohberger, B., Stuendl, N., Glaenzer, D. (2020). CoCrMo surface modifications affect biocompatibility, adhesion, and inflammation in human osteoblasts. *Sci Rep,* 10, 1682. https://doi.org/10.1038/s41598-020-58742-9.

17. Pröbster, L., Voigt, C., Fuhrmann, G. (1994). Tensile and torsional shear strength of the bone implant interface of titanium implants in the rabbit. *J Mater Sci: Mater Med,* 5, 314–319. https://doi.org/10.1007/BF00058954

18. Masuda, T., Yliheikkilä, P. K., Felton, D. A., & Cooper, L. F. (1998). Generalizations regarding the process and phenomenon of osseointegration. Part I. In vivo studies. *The International journal of oral & maxillofacial implants*, *13*(1), 17–29.

19. Tarala, M., Waanders, D., Biemond, J. E., Hannink, G., Janssen, D., Buma, P., & Verdonschot, N. (2011). The effect of bone ingrowth depth on the tensile and shear strength of the implant-bone e-beam produced interface. *Journal of materials science. Materials in medicine*, *22*(10), 2339–2346. https://doi.org/10.1007/s10856-011-4419-z

20. Carpenter, R. D., Klosterhoff, B. S., Torstrick, F. B., Foley, K. T., Burkus, J. K., Lee, C., Gall, K., Guldberg, R. E., & Safranski, D. L. (2018). Effect of porous orthopaedic implant material and structure on load sharing with simulated bone ingrowth: A finite element analysis comparing titanium and PEEK. *Journal of the mechanical behavior of biomedical materials*, *80*, 68–76. https://doi.org/10.1016/j.jmbbm.2018.01.017

21. Klokkevold, P. R., Johnson, P., Dadgostari, S., Caputo, A., Davies, J. E., & Nishimura, R. D. (2001). Early endosseous integration enhanced by dual acid etching of titanium: a torque removal study in the rabbit. *Clinical oral implants research*, *12*(4), 350–357. https://doi.org/10.1034/j.1600-0501.2001.012004350.x

22. Gittens, R. A., Olivares-Navarrete, R., Schwartz, Z., & Boyan, B. D. (2014). Implant osseointegration and the role of microroughness and nanostructures: lessons for spine implants. *Acta biomaterialia*, *10*(8), 3363–3371. https://doi.org/10.1016/j.actbio.2014.03.037

23. Cheng, B. C., Koduri, S., Wing, C. A., Woolery, N., Cook, D. J., & Spiro, R. C. (2018). Porous titanium-coated polyetheretherketone implants exhibit an improved bone-implant interface: an in vitro and in vivo biochemical, biomechanical, and histological study. *Medical devices (Auckland, N.Z.)*, *11*, 391–402. https://doi.org/10.2147/MDER.S180482

24. Wong, M., Eulenberger, J., Schenk, R., & Hunziker, E. (1995). Effect of surface topology on the osseointegration of implant materials in trabecular bone. *Journal of biomedical materials research*, *29*(12), 1567–1575. https://doi.org/10.1002/jbm.820291213

25. Buser, D., Schenk, R. K., Steinemann, S., Fiorellini, J. P., Fox, C. H., & Stich, H. (1991). Influence of surface characteristics on bone integration of titanium implants. A histomorphometric study in miniature pigs. *Journal of biomedical materials research*, *25*(7), 889–902. https://doi.org/10.1002/jbm.820250708

26. W. Winkler-Gniewek. (1989). *PLASMAPORE® coating for cement-free bonding of joint endoprostheses*. Tuttlingen, Baden-Württemberg, Germany; B. Braun.

27. Salito, A. (2016). In *Implant Surface Functionalities for Improved Biocompatibility Plasmapore XP™ Coating* (pp. 1–80). Baden-Dättwil, Switzerland; Orchid Orthopedic Solutions.
28. *Our Facilities.* (n.d.). Retrieved from Lehigh University CENTER FOR ADVANCED MATERIALS & NANOTECHNOLOGY: https://www.lehigh.edu/nano/facilities.html
29. *Alpha-Step D-500.* (n.d.). Retrieved from KLA: https://www.kla-tencor.com/products/instruments/stylus-profilers/alphastep-d-500
30. Butner, S. (2017, April 24). *How to Calculate the Time for Cell Doubling.* Retrieved from Sciencing: https://sciencing.com/calculate-time-cell-doubling-8219903.html
31. Ashour, M. B., Gee, S. J., & Hammock, B. D. (1987). Use of a 96-well microplate reader for measuring routine enzyme activities. *Analytical biochemistry*, *166*(2), 353–360. https://doi.org/10.1016/0003-2697(87)90585-9
32. Jain, R. Wang, S., Moawad, H., Falk, M., & Jain, H. (2009) Glass Bone Implants: The Effect of Surface Topology on Attachment and Proliferation of Osteoblast Cells on 45S Bioactive Glass. *MRS Online Proceedings Library*, 1235, 347. 10.1557/PROC-1235-RR03-47
33. Le Guéhennec, L., Soueidan, A., Layrolle, P., & Amouriq, Y. (2007). Surface treatments of titanium dental implants for rapid osseointegration. *Dental materials: official publication of the Academy of Dental Materials*, *23*(7), 844–854. https://doi.org/10.1016/j.dental.2006.06.025
34. Knothe Tate, M. L., Adamson, J. R., Tami, A. E., & Bauer, T. W. (2004). The osteocyte. *The international journal of biochemistry & cell biology*, *36*(1), 1–8.

https://doi.org/10.1016/s1357-2725(03)00241-3

35. Prokharau, P. A., Vermolen, F. J., & García-Aznar, J. M. (2012). Model for direct bone apposition on pre-existing surfaces, during peri-implant osseointegration. *Journal of theoretical biology*, *304*, 131–142. https://doi.org/10.1016/j.jtbi.2012.03.025
36. Du, Z., Ivanovski, S., Hamlet, S. M., Feng, J. Q., & Xiao, Y. (2016). The Ultrastructural Relationship Between Osteocytes and Dental Implants Following Osseointegration. *Clinical implant dentistry and related research*, *18*(2), 270–280. https://doi.org/10.1111/cid.12257
37. Althaus, J., Padeste, C., Köser, J., Pieles, U., Peters, K., & Müller, B. (2012). Nanostructuring polyetheretherketone for medical implants. *European Journal of Nanomedicine*, *4*(1), 7-15.
38. Novotna, Z., Reznickova, A., Rimpelova, S., Vesely, M., Kolska, Z., & Svorcik, V. (2015). Tailoring of PEEK bioactivity for improved cell interaction: plasma treatment in action. *RSC Advances*, 5, 41428-41436. 10.1039/C5RA03861H
39. Ruijtenberg, S., & van den Heuvel, S. (2016). Coordinating cell proliferation and differentiation: Antagonism between cell cycle regulators and cell type-specific gene expression. *Cell cycle (Georgetown, Tex.)*, *15*(2), 196–212. https://doi.org/10.1080/15384101.2015.1120925
40. Thermo Scientific Nunc Adherent Cell Culture Surface, https://www.thermofisher.com/us/en/home/life-science/cell-culture/cell-culture-plastics/nunc-adherent-cell-culture-surface.html?ef_id=Cj0KCQjwppSEBhCGARIsANIs4p7yGyMShO3VMWBqi10Z94a5RHEOZ7biPj0qg_VOieAg4UjI-R1z_jAaAj7LEALw_wcB:G:s&s_kwcid=AL!3652!3!413877634467!e!!g!!nunclon%

20delta%20surface&cid=bid_clb_ccp_r01_co_cp0000_pjt0000_bid00000_0se_gaw_bt_pur_con&gclid=Cj0KCQjwppSEBhCGARIsANIs4p7yGyMShO3VMWBqi10Z94a5RHEOZ7biPj0qg_VOieAg4UjI-R1z_jAaAj7LEALw_wcB

41. Sartoretto, S. C., Alves, A. T., Resende, R. F., Calasans-Maia, J., Granjeiro, J. M., & Calasans-Maia, M. D. (2015). Early osseointegration driven by the surface chemistry and wettability of dental implants. *Journal of applied oral science : revista FOB*, *23*(3), 279–287. https://doi.org/10.1590/1678-775720140483
42. Foppiano, S., Marshall, S. J., Marshall, G. W., Saiz, E., & Tomsia, A. P. (2007). Bioactive glass coatings affect the behavior of osteoblast-like cells. *Acta biomaterialia*, *3*(5), 765–771. https://doi.org/10.1016/j.actbio.2007.02.011
43. Foppiano, S., Marshall, S. J., Marshall, G. W., Saiz, E., & Tomsia, A. P. (2004). The influence of novel bioactive glasses on in vitro osteoblast behavior. *Journal of biomedical materials research. Part A*, *71*(2), 242–249. https://doi.org/10.1002/jbm.a.30159
44. Ratner, B. D. (2004). **Biomaterials science: An introduction to materials in medicine**. Amsterdam: Elsevier Academic Press.
45. Tomsia, A., Saiz, E., Song, J. & Bertozzi, C. (2005), Biomimetic Bonelike Composites and Novel Bioactive Glass Coatings. *Adv. Eng. Mater.*, 7, 999-1004. https://doi.org/10.1002/adem.200500143
46. Hench, L.L. (1991), Bioceramics: From Concept to Clinic. *Journal of the American Ceramic Society*, 74, 1487-1510. https://doi.org/10.1111/j.1151-2916.1991.tb07132.x
47. Oliver, J. N., Su, Y., Lu, X., Kuo, P. H., Du, J., & Zhu, D. (2019). Bioactive glass coatings on metallic implants for biomedical applications. *Bioactive materials*, *4*, 261–270. https://doi.org/10.1016/j.bioactmat.2019.09.002

48. Gomez-Vega, J. M., Saiz, E., Tomsia, A. P., Marshall, G. W., & Marshall, S. J. (2000). Bioactive glass coatings with hydroxyapatite and Bioglass particles on Ti-based implants. 1. Processing. *Biomaterials*, *21*(2), 105–111. https://doi.org/10.1016/s0142-9612(99)00131-3

49. Wang, S., Kowal, T. J., Marei, M. K., Falk, M. M., & Jain, H. (2013). Nanoporosity significantly enhances the biological performance of engineered glass tissue scaffolds. *Tissue engineering. Part A*, *19*(13-14), 1632–1640. https://doi.org/10.1089/ten.TEA.2012.0585

50. Kowal, T. J., Hahn, N. C., Eider, S., Marzillier, J. Y., Fodera, D. M., Thamma, U., Jain, H., & Falk, M. M. (2018). New bioactive glass scaffolds with exceptional qualities for bone tissue regeneration: response of osteoblasts and osteoclasts. *Biomedical materials (Bristol, England)*, *13*(2), 025005. https://doi.org/10.1088/1748-605X/aa9385

51. Thamma, U., Kowal, T., Falk, M., & Jain, H. (2019). Influence of nanoporosity on the nature of hydroxyapatite formed on bioactive calcium silicate model glass. *Journal of biomedical materials research. Part B, Applied biomaterials*, *107*(4), 886–899. https://doi.org/10.1002/jbm.b.34184

52. Foppiano, S., Marshall, S. J., Saiz, E., Tomsia, A. P., & Marshall, G. W. (2006). Functionally graded bioactive coatings: reproducibility and stability of the coating under cell culture conditions. *Acta biomaterialia*, *2*(2), 133–142. https://doi.org/10.1016/j.actbio.2005.12.003

53. Stadlinger, B., Pilling, E., Huhle, M., Mai, R., Bierbaum, S., Bernhardt, R., Scharnweber, D., Kuhlisch, E., Hempel, U., & Eckelt, U. (2007). Influence of extracellular matrix coatings on implant stability and osseointegration: an animal study. *Journal of biomedical materials research. Part B, Applied biomaterials*, *83*(1), 222–231. https://doi.org/10.1002/jbm.b.30787

54. Varoni, E., Canciani, E., Palazzo, B., Varasano, V., Chevallier, P., Petrizzi, L., Dellavia, C., Mantovani, D., & Rimondini, L. (2015). Effect of Poly-L-Lysine coating on titanium osseointegration: from characterization to in vivo studies. *The Journal of oral implantology*, *41*(6), 626–631. https://doi.org/10.1563/AAID-JOI-D-13-00036

55. Schwartz, Z., Raz, P., Zhao, G., Barak, Y., Tauber, M., Yao, H., & Boyan, B. D. (2008). Effect of micrometer-scale roughness of the surface of Ti6Al4V pedicle screws in vitro and in vivo. *The Journal of bone and joint surgery. American volume*, *90*(11), 2485–2498. https://doi.org/10.2106/JBJS.G.00499

56. Varanasi, V. G., Saiz, E., Loomer, P. M., Ancheta, B., Uritani, N., Ho, S. P., Tomsia, A. P., Marshall, S. J., & Marshall, G. W. (2009). Enhanced osteocalcin expression by osteoblast-like cells (MC3T3-E1) exposed to bioactive coating glass (SiO2-CaO-P2O5-MgO-K2O-Na2O system) ions. *Acta biomaterialia*, *5*(9), 3536–3547. https://doi.org/10.1016/j.actbio.2009.05.035

57. Woo E. J. (2012). Recombinant human bone morphogenetic protein-2: adverse events reported to the Manufacturer and User Facility Device Experience database. *The spine journal: official journal of the North American Spine Society*, *12*(10), 894–899. https://doi.org/10.1016/j.spinee.2012.09.052

58. Yirka, B. (2021, April 6). *Newly identified protein enables cells to sense surroundings and anchor in the right places.* Retrieved from Phys.org: Cell & Microbiology, Molecular & Computational Biology: https://phys.org/news/2021-04-newly-protein-enables-cells-anchor.html#:~:text=The%20protein%20is%20called%20paxillin,sensory%20information%20about%20nearby%20material

59. Turner, C. E., Glenney, J. R., Jr, & Burridge, K. (1990). Paxillin: a new vinculin-binding protein present in focal adhesions. *The Journal of cell biology*, *111*(3), 1059–1068. https://doi.org/10.1083/jcb.111.3.1059

60. Castillo, A. B., Blundo, J. T., Chen, J. C., Lee, K. L., Yereddi, N. R., Jang, E., Kumar, S., Tang, W. J., Zarrin, S., Kim, J. B., & Jacobs, C. R. (2012). Focal adhesion kinase plays a role in osteoblast mechanotransduction in vitro but does not affect load-induced bone formation in vivo. *PloS one*, *7*(9), e43291. https://doi.org/10.1371/journal.pone.0043291

61. Young, E. W., & Beebe, D. J. (2010). Fundamentals of microfluidic cell culture in controlled microenvironments. *Chemical Society reviews*, *39*(3), 1036–1048. https://doi.org/10.1039/b909900j

Michael Levin

mil619@lehigh.edu

(267) 648-8189

Present Address
2411 Diane's Way
Warrington, PA 18976

Permanent Address
2411 Diane's Way
Warrington, PA 18976

Citizenship: U.S. Citizen

Education:

Undergraduate:
Temple University, Philadelphia, PA
Bachelor of Science in Biochemistry, GPA: 3.63, May 2015

Graduate:
Lehigh University, Bethlehem, PA
Master of Science in Bioengineering, GPA: 3.47, May 2021

Research Experiences:

Bioengineering/Materials Science & Engineering/Biological Sciences Department, Lehigh University, Bethlehem, PA

Master's thesis
Graduate Student/Research Assistant, August 2019 – present
Supervisors: Dr. Himanshu Jain and Dr. Matthias Falk, Principal Investigators

Biomaterials Research, specializing on the field of *Spinal Implants*.

- Spine implant's surface topology and elemental composition analysis, along with testing implant's effects on bone cell's attachment, proliferation, and differentiation rate.
- Working independently on Wet Lab, Material Science, and Microscopic Bench work.
- Cell Culture Maintenance.
- Protocol Development.
- Running and developing assays for quantitative measurements.
- Running scanning electron microscope for surface characterization analysis.
- Running energy dispersive spectroscopy for surface, elemental composition analysis.
- Running optical microscopes for visually seeing bone cells' morphology and their secreted biomolecules.

National Institute of Biomedical Imaging and Bioengineering, National Institutes of Health, Bethesda, MD

Post-baccalaureate IRTA Research Fellow, March 2017 – March 2019
Supervisor: Dr. Hari Shroff, Senior Investigator

Advanced Microscopy Research, specializing on the field of *Optical Resolution and Fluorescence Imaging*.

- Acquiring, untwisting, and tracking *C. Elegan*'s cellular imaging for anatomical, 4D mapping.

- Working independently, as well as in group setting, on Wet Lab, Computational, and Microscopic Bench work.
- Screening strains for potential tracking.
- Running optical images through diSPIM microscope.
- Manipulating optical images through computer programming.

Department of Molecular Therapeutics, Fox Chase Cancer Center, Philadelphia, PA

Research Associate, June 2015 – April 2016
Supervisor: Dr. Elizabeth Hopper-Borge, Principal Investigator

Biochemistry Research, specializing on the field of *Proteomics*.

- Testing an inhibitor's effect on cancer cell's ABC Transporters for determining inhibition success on that protein, and to identify its therapeutic, binding sites.
- Worked independently on Wet Lab Bench work.
- Improved protocols for more efficient results.
- Analyzed peptide mass fingerprinting on ABCC10.

Department of Bioengineering, Temple University, Philadelphia, PA

Undergraduate Student/Research Assistant, August 2014 – May 2015
Supervisor: Dr. Omar Fischer, Assistant Professor

Pharmaceutical Research, specializing on the field *of Nanomedicine.*

- Development and synthesis of novel pH-responsive nanoparticles for targeted, intracellular delivery of therapeutics towards cancer cells.
- Worked independently, as well as in group setting, on Wet Lab Bench work.
- Included alteration of nanoparticulate surface coatings, core hydrophobicity, and novel cancer cell targeting schemes.

Honors and Awards:

Kramer Memorial Fund, 2013
Dean's List, 2011 – 2013
Cum Laude, 2015
Distinction in Major, 2015

Presentations:

Oral Presentations:

- **Postbac Seminar Series, National Institutes of Health**, Constructing a 4D Atlas of *Caenorhabditis elegans* embryogenesis post-twitching, Jan. 2018
- **Baltimore Worm Club, University of Maryland, Baltimore County (UMBC)**, Creating an Atlas of Nuclear Positions in the *Caenorhabditis elegans* embryo, Nov. 2018

Poster Presentations:

- **NIH Postbac Poster, National Institutes of Health**, Creating a 4D Nuclear Atlas in Embryonic *Caenorhabditis elegans,* May 2018
- **63rd Annual Biophysical Society Meeting, Baltimore, Maryland**, Generating a 4D Atlas of Nuclear Positions in Embryonic *Caenorhabditis elegans*, Mar. 2019